Quantifying the influence of biophysical factors in shaping brain communication through remnant functional networks

Johan Nakuci[1,*], Javier Garcia[1], and Kanika Bansal[1,2,*]

[1]U.S. Army DEVCOM Army Research Laboratory, Aberdeen Proving Ground, Aberdeen, MD, 21005, USA

[2]Computer Science and Electrical Engineering, University of Maryland Baltimore County, Baltimore, MD, 21250, USA

*Corresponding authors' Emails: jnakuci@gmail.com; phy.kanika@gmail.com

Competing Interest Statement: The authors declare no competing interests.

Keywords: functional connectivity, structural connectivity, spatial auto-correlation, neuroreceptors, neuropsychiatric illness

Acknowledgements: This research was supported by the U.S. Army DEVCOM Army Research Laboratory through mission funding (JOG) and army educational outreach program (KB, JN, W911SR-15-2-0001). The views and conclusions contained in this document are those of the authors and should not be interpreted as representing the official policies, either expressed or implied, of the U.S. Army DEVCOM Army Research Laboratory or the U.S. Government. The U.S. Government is authorized to reproduce and distribute reprints for Government purposes notwithstanding any copyright notation herein.

Author Contributions

Conceptualization: JN, KB
Data Curation: JN
Formal analysis: JN
Funding acquisition: JOG, KB
Methodology: JN, KB
Supervision: KB, JOG
Visualization: JN, KB
Writing – original draft: JN, KB
Writing – review & editing: JN, JOG, KB

Abstract

Functional connectivity (FC) reflects brain-wide communication crucial for cognition, yet the role of underlying biophysical factors, physical and molecular, in shaping FC remains unclear. We quantify the influence of physical factors—structural connectivity (SC) and spatial autocorrelation (DC), capturing anatomical wiring and distance between regions—and molecular factors—gene expression similarity (GC) and neuroreceptor congruence (RC), capturing similarity in the neurobiological make up—on the organizational features of fMRI derived resting-state FC. We assess the impact of these factors on graph-theoretic and topological features, capturing both pairwise and higher-order interactions between brain regions. We develop a simple test using *remnant functional network*s generated by selectively removing connections aligned with specific biophysical factors. Our findings reveal that molecular factors, particularly RC, predominantly shape graph-theoretic features, while topological features are influenced by a mix of molecular and physical factors, notably GC and DC. Surprisingly, SC plays a minor role in FC organization. Additionally, we link FC alterations to specific biophysical factors in neuropsychiatric conditions such as schizophrenia, bipolar disorder, and ADHD, with physical factors more effectively differentiating these groups. These insights are crucial for understanding and modeling FC across various applications. Our analysis offers a robust method to examine how underlying factors dynamically influence FC in different contexts beyond resting state, including during a task, development, and clinical conditions.

Introduction

Communication among brain regions is fundamental to function. Functional connectivity (FC) provides a compact view of the fundamental features of brain-wide communication[1] essential for cognitive processes[2,3]. However, how the features of FC, and intrinsically linked regional brain communication, emerge from the underlying biophysical constraints is poorly understood.

These features have been primarily investigated using graph-theoretic measures which quantify pairwise relationships between brain regions. Graph-theoretic measures have identified components facilitating efficient information transfer[4], global integration and local segregation[5], and robustness to injury crucial for effective communication[6]. Additionally, recent work has shown that alongside pairwise relationships, higher-order interactions associated with the topology of the FC network, are also a fundamental feature of brain communication[7]. Here we uncover how the features of the brain's functional connectivity network are constrained by fundamental interactions in the brain.

Most studies and modeling frameworks have focused on understanding the role of anatomical wiring or structural connectivity (SC) in constraining FC, which provides a fundamental *physical* basis for brain communication[8]. Nonetheless, other factors have been shown to shape brain-wide communication. Another physical factor is spatial auto-correlation (distance dependent connectivity or DC) which inherently allows for easier and/or faster communication between regions that are in closer proximity than the ones at farther physical distance[8]. Brain communication is also fundamentally constrained and shaped by molecular relationships which reflect the similarity in the neurobiological make-up of the regions. Previous studies have captured these relationships using similarity in genetic expression (GC)[10] and neuroreceptor density (RC)[10], between two brain regions. Here we consider these *biophysical factors* collectively to uncover the extent to which physical and molecular factors constrain and shape the fundamental features of FC.

We developed a simple test to quantify the underlying influence of biophysical factors. First, for each of the biophysical factors we derive a corresponding biophysical network that quantifies the pairwise relationship between brain regions. Then we compute the alteration in organizational

features of the FC network before and after the connections shared by a reference biophysical network are removed. We call these FC connectivity maps with removed connections *remnant functional networks* (RFNs; **Fig. 1**). Observed differences between the organizational features of the FC and various RFNs inform us on how a biophysical network shapes FC.

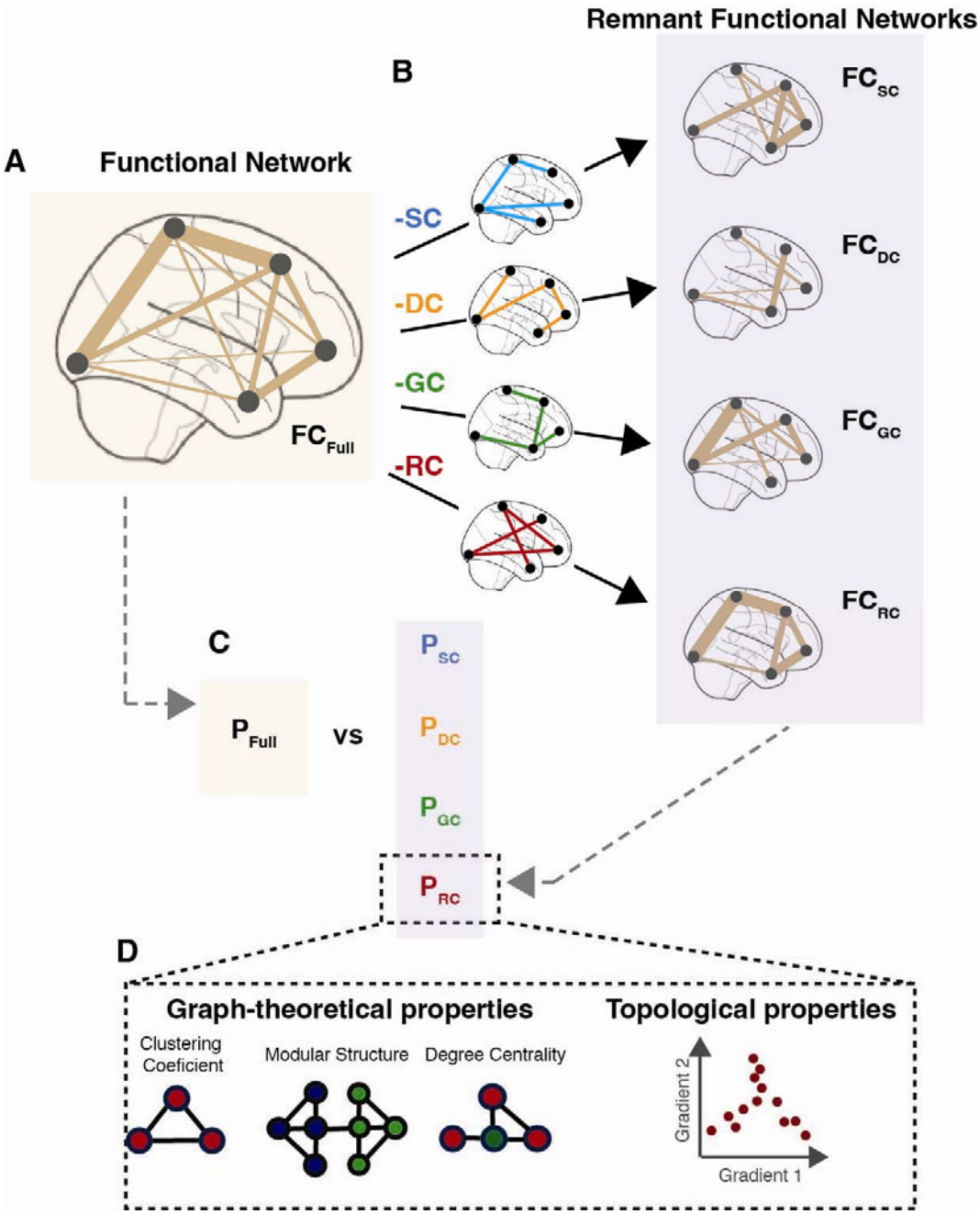

Figure 1. Schematic of the analytical test based on remnant functional networks. (A) Fully connected weighted functional connectivity network (FC_{Full}). The width of the lines represents the strength of the connection. (B) We derive remnant functional networks (RFNs) by removing

the connections in FC_{Full} that share a direct connection in an underlying biophysical network. These biophysical networks are structural connectivity (SC), spatial auto-correlation (DC), similarity in genetic expression (GC) and neuroreceptor congruence (RC) between brain regions; and corresponding RFNs are denoted by FC_{SC}, FC_{DC}, FC_{GC}, and FC_{RC} respectively. (C) To assess the role of these biophysical networks in shaping the organization of the brain's functional connectivity, we compare the features (P) of FC_{SC}, FC_{DC}, FC_{GC}, and FC_{RC} (i.e., P_{SC}, P_{DC}, P_{GC}, and P_{RC}) with the features of FC_{Full} (i.e., P_{Full}). (D) The features we employ comprise a comprehensive set of graph-theoretical and topological metrics.

We present our main findings with functional connectivity and RFNs obtained from the Human Connectome Project (HCP)[12], and also corroborate them in another publicly available dataset UCLA Consortium for Neuropsychiatric Phenomics Dataset (LA5c)[13]. Additionally, we complement our analytical test with a modeling analysis that predicts functional connectivity from each of the biophysical networks. Lastly, we extend the framework to understand disease specific alterations, particularly neuropsychiatric disorders where deviations in connectivity patterns are likely subtle, to identify the biophysical networks contributing to cognitive disturbances.

Results

<u>Reference functional connectivity and biophysical networks</u>

The analysis aims to quantify the influence different biophysical networks have in constraining and shaping the foundational organization of brain functional connectivity estimated from fMRI derived BOLD signal. To accomplish this, we first estimated the functional connectivity for an individual subject from the Human Connectome Project (HCP, N=48), using the resting-state fMRI signal from 200 brain regions derived from the Schaefer atlas, and computing the Pearson correlation between pairs of brain regions[14]. We then average FC networks across individuals to derive the reference functional connectivity – FC_{Full} (**Fig. 1A and Fig. 2A**).

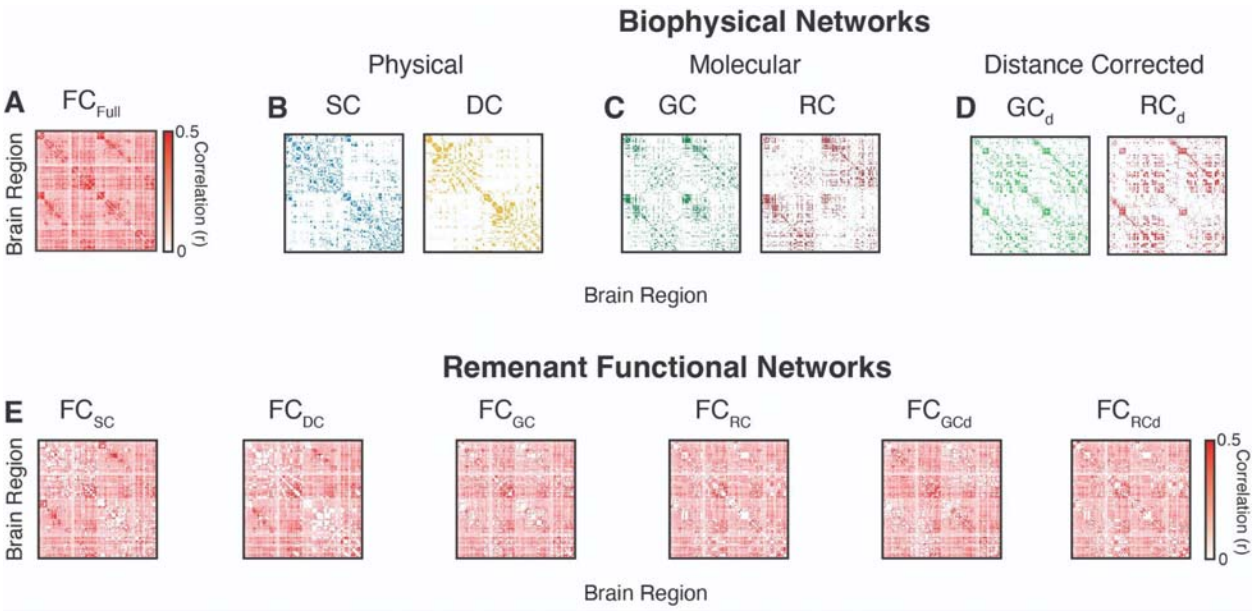

Figure 2. Connectivity patterns of group-level FC, SC, DC, GC and RC networks. (A) Functional brain connectivity (FC_{Full}) between 200 brain regions derived from the Schaefer brain atlas. (B) structural connectivity (SC, *left*) and spatial auto-correlation (DC, *right*), networks reflecting physical constraints between brain regions. (C) Similarity in gene expression (GC, *left*) and neuroreceptor congruence (RC), networks reflecting molecular relationships between brain regions. (D) Distance corrected gene expression (GC_{ED}, *left*) and neuroreceptor congruence (RC_{ED}, *left*). (E) Remnant functional networks derived from each of the biophysical networks – FC_{SC}, FC_{DC}, FC_{GC}, FC_{RC}, FC_{GCd}, and FC_{RCd}**.**

As described in **Fig.1**, our test used FC_{Ful} to construct remnant functional networks (RFNs) by removing edges shared with a given biophysical network (**Fig. 1B**). We then estimated several features of FC_{Full} and for each RFNs to quantify and compare the effect of a biophysical factor on a given network feature (**Fig. 1C**). We employed a variety of graph-theoretical as well as topological features, capturing pair-wise as well as higher-order interactions, to gain a holistic understanding of the role of different biophysical factors (**Fig. 1D**).

Reference biophysical networks that reflect a diverse array of relationships between two brain regions were derived differently. We focus on two groups–physical and molecular networks– where physical networks reflect either the physical wiring or physical distance between two brain regions. To capture physical wiring, we derived group-level structural connectivity (SC) from white matter streamlines (**Fig. 2B**). To capture distance-based relationships, we derived

distance dependent connectivity (DC) by computing Euclidean distance between the centroids of two corresponding brain regions in the Schaefer atlas (**Fig. 2B**).

For molecular relationships we focused on two distinct neurobiological factors pertaining to the regional similarities in gene expression (GC) and neuroreceptor density (RC). GC or the extent to which two brain regions express the same genes, was estimated from RNA microarray data using the Pearson correlation (**Fig. 2C**)[15]. Similarly, RC or the extent to which two brain regions exhibit similar concentration of neuroreceptors was estimated from PET tracer imaging of 19 neuroreceptors and transporters maps using the Pearson correlations (**Fig. 2C**)[11]. Additionally, previous work has shown that the similarity in genetic expression and neuroreceptor congruence is dependent on the distance between brain regions[9]. To account for this dependence, we derived two additional distance corrected networks – GC_d and RC_d (**Fig. 2D,** see Methods for more details on molecular networks).

SC is a sparsely connected network due to the absence of a direct anatomical connection between several brain regions; other factors represent fully connected networks, meaning, a nonzero value connects all pairs of regions. This mismatch in the *density* of the networks does not allow for a comparison across different biophysical networks. Therefore, we matched the density of all the biophysical networks (DC, GC, RC) to SC ensuring that the same number of connections were removed when constructing the RFNs (see Methods). **Fig. 2E** shows the RFNs created by removing connections associated with different biophysical networks in FC_{Full}. In the following sections we utilize RFNs to quantify the influence each of the biophysical networks has on the organization of functional brain connectivity.

<u>Biophysical networks constraining and shaping graph-theoretical features of FC</u>

First, we focus on determining how biophysical networks shape pairwise relationships between brain regions by quantifying the changes in graph-theoretic features between FC_{Full} and RFNs. We leveraged a comprehensive set of features that have been identified to measure a diverse set of functions required for cognitive processing[16]. These features include modularity, weighted degree, clustering coefficient, path length, spectral radius, eigenvector centrality, and synchronizability (see methods for details). Specifically, we calculated each of these features for

the group-level functional connectivity network (P_{Full}) and then assessed the percent changes in each of these features in the RFNs. Evaluating percent change allowed us to compare the relative shift in different features despite the differences in their magnitude.

Comparing across graph-theoretic measures, removing shared connections with biophysical networks affected modularity the most (|Δ| = 24.27 ± 10.53% on an average; **Fig. 3A**). Modularity was followed by spectral radius, clustering coefficient, and weighted degree (~ 20% change on average). Whereas eigenvector centrality showed the lowest change (< 1%). Across all graph-theoretic properties, the molecular networks, particularly RC, were the dominant factor. On average RC had the strongest impact (i.e. |Δ|) of 18.66 ± 10.70%; **Fig. 3B**). Even after correcting for the distance dependencies, RC_d had a higher impact than the other biophysical networks (|Δ| = 17.59 ± 9.75%). Moreover, the GC network closely followed the magnitude of RC in shaping FC. Interestingly, removing SC associated connections had the least effect on the organization of FC compared to all other biophysical networks.

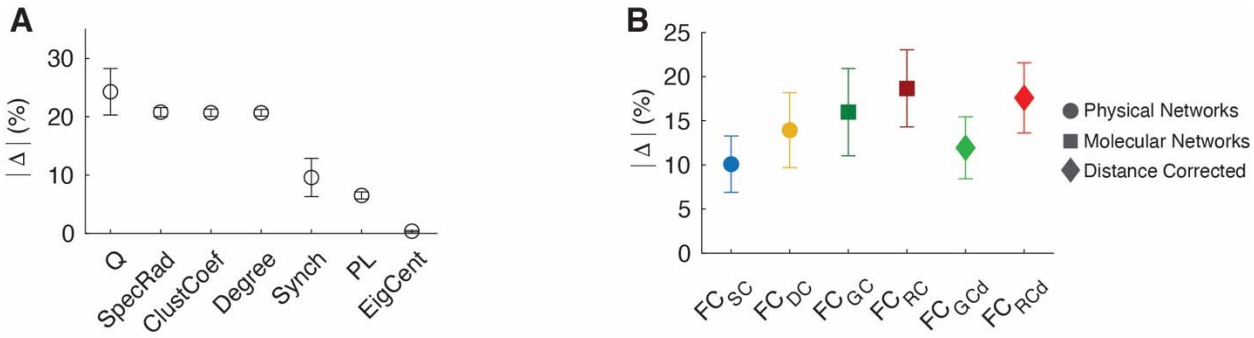

Figure 3. Molecular networks are the dominant factor constraining and shaping functional connectivity. (A) Average change in graph-theoretic metrics across biophysical networks. Weighted Degree (Degree), Clustering Coefficient (ClustCoef), Spectral Radius (SpecRad), Path Length (PL), Modularity (Q), Synchronizability (Synch) and Eigenvector Centrality (EigCent). (B) Average change for biophysical networks across graph-theoretic metrics, highlighting the dominance of molecular networks and RC in particular.

Focusing on individual graph-theoretic properties, as can be observed in **Fig. 4A**, for weighted degree removing connections associated with each of the biophysical networks, resulted in a decrease in weighted degree in the RFNs compared to FC_{Full}. The largest change occurred due to molecular factors – FC_{RC} (Δ = -22.07%) and FC_{GC} (Δ = -21.24%), followed by FC_{DC} (Δ = -20.39%), and FC_{SC} (Δ = -17.99%). Moreover, we found that correcting for distance in RC and

GC had a similar effect – FC_{RCd} (Δ = -22.08%), FC_{GCd} (Δ = -20.29%). Overall, neuroreceptor congruence emerged as a pivotal factor affecting weighted degree.

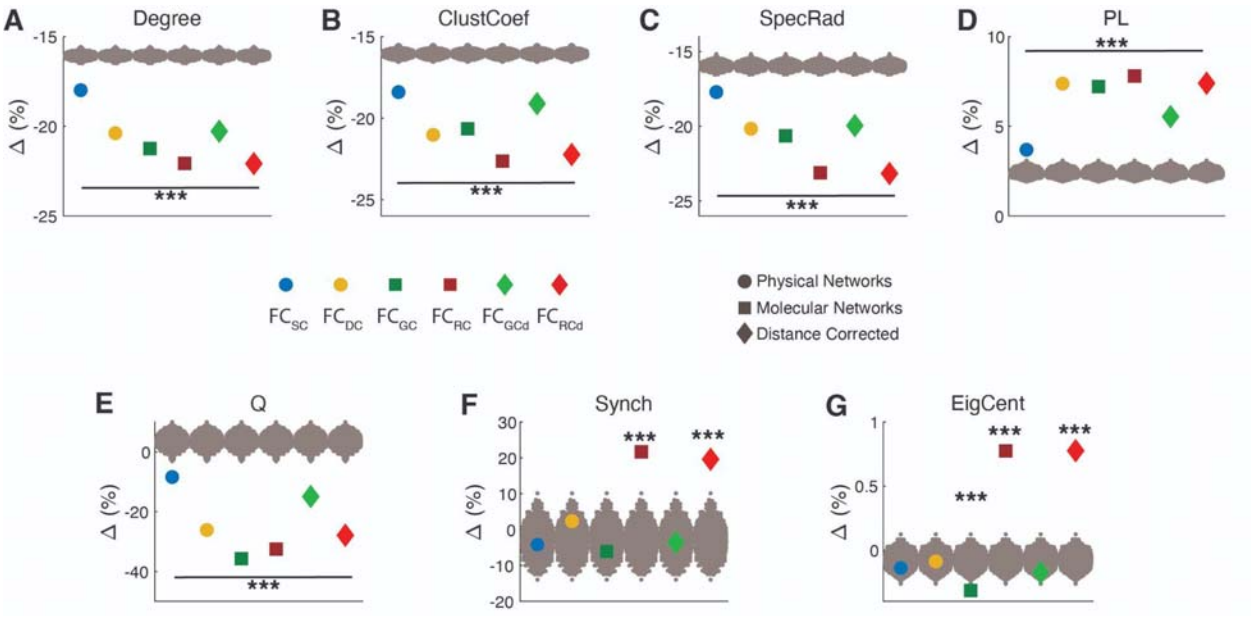

Figure 4. Biophysical networks shaping the graph-theoretical properties of functional brain connectivity. (A) Weighted Degree (Degree), (B) Clustering Coefficient (ClustCoef), (C) Spectral Radius (SpecRad), (D) Path Length (PL), (E) Modularity (Q), (F) Synchronizability (Synch) and (G) Eigenvector Centrality (EigCent). The effect of each biophysical network was quantified as a percent change (Δ) between FC_{Full} and RFNs for each graph-theoretic measure. Colored dots represent the values after removing SC, DC, GC, RC, GC_d, and RC_d associated connections in the FC_{Full}. Gray dots represent the values after removing a random set of connections in the FC_{Full} (null model). FC_{SC}: FC with SC associated connections removed; FC_{DC}: FC with DC connections removed; FC_{GC}: FC with GC connections removed; FC_{RC}: FC with RC connections removed; FC_{GCd}: FC with GC corrected for distance dependencies removed; FC_{RCd}: FC with RC corrected for distance dependencies removed. Statistical testing assessed the deviation from the null model with *** denoting p-value < 0.001.

The weighted degree of the network, and other network properties, will inherently change when connections are removed, therefore, we tested if the observed changes were greater than what would be observed from removing random connections – null model. We randomly removed a set of connections from FC_{Full} that were equal to the number of connections removed by each of the biophysical networks and calculated the shift in graph-theoretic features. This procedure was repeated 1,000 times to generate a null distribution. The observed alterations in weighted degree

induced by each of the biophysical networks were significantly greater than the null model ($P_{rand} < 0.001$).

Similarly, we observed the dominance of molecular factors on other network features. Particularly, RC-based networks (FC_{RC}) exerted the dominant influence on average clustering coefficient (Δ = -22.64%, $P_{rand} < 0.001$; **Fig. 4B**), spectral radius (Δ = -23.16%, $P_{rand} < 0.001$; **Fig. 4C**) and path length (Δ = 7.80%, $P_{rand} < 0.001$; **Fig. 4D**). For modularity, GC-based network exerted the strongest influence (FC_{GC}: Δ = -35.72%; $P_{rand} < 0.001$) closely followed by RC-based networks (FC_{RC}: Δ = -32.56%; $P_{rand} < 0.001$); however, after correcting for distance, RC exerted the larger influence (FC_{RCd}: Δ = -27.91%; $P_{rand} < 0.001$; **Fig. 4E**). Moreover, RC-based networks similarly exerted the largest influence on synchronizability – FC_{RC} (Δ = 21.67%, $P_{rand} < 0.001$; **Fig. 4F**), and eigenvector centrality – FC_{RC} (Δ = 0.78%, $P_{rand} < 0.001$; **Fig. 4G**).

In general, we observed a higher influence of molecular factors than physical factors, with structural connectivity showing the lowest percent change in all the graph-theoretic metrics tested. These results suggest that attempting to derive functional relationships from structural connections only has severe limitations and instead a greater emphasis should be placed on molecular factors (i.e. genetic expression and neuroreceptor congruence).

<u>Regional relationship between biophysical factors and graph-theoretic features of FC</u>

Given the dominance of neuroreceptors congruence, we additionally probed the regional specificity of RC driven changes for graph-theoretic properties for which a value could be estimated for each brain region, i.e., weighted degree, eigenvector centrality, and clustering coefficient. For this analysis, percent change in these node-wise features was calculated at the region level and in Fig. 5 we show the observed changes as a brain-wide heat map. We found that the relationship between neuroreceptor congruence and these features was differentially distributed across the cortex. In particular, neuroreceptor congruence induced the largest shifts in the dorsolateral prefrontal cortex, motor and visual areas, whereas the medial prefrontal cortex and insula exhibited minor changes. It is worth noting, that while on average neuroreceptor congruence exhibited minimal effect on eigenvector centrality (**Fig. 4G**), this was a result of the differential relationship across the cortex (**Fig. 5C**). In fact, removing RC driven connectivity led

to an increase in the eigenvector centrality of the medial prefrontal cortex, parietal cortex, insula and temporal lobe suggesting that neuroreceptor congruence functions to dampen the centrality profile of these brain regions. Moreover, the magnitude of change across brain regions for weighted degree and clustering coefficient is strongly associated with strength of the feature indicating that the hub properties emerge from underlying neuroreceptor congruence (**Fig. 5D, Fig. S1**).

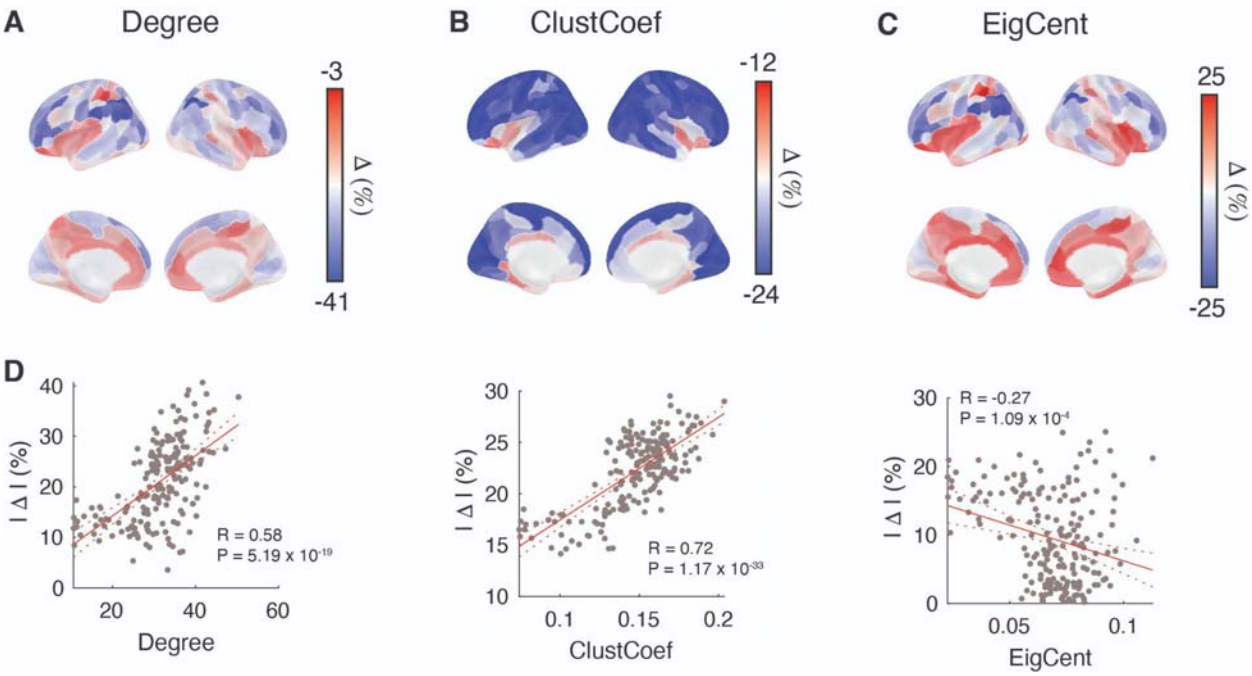

Figure 5. Neuroreceptor congruence dependent associations in functional connectivity are brain wide. Impact of neuroreceptor congruence on (A) weighted degree, (B) clustering coefficient, and (C) eigenvector centrality across the cortex. (D) Relationship between the regional network features and magnitude of change across brain regions.

<u>Biophysical networks constraining and shaping the topological organization of FC</u>

In addition to graph-theoretic features which focus on pairwise relationships between brain regions, topological analysis can be used to infer higher-order relationships among brain regions. The topological architecture of the cortex is one of the organizational features that is believed to anchor cortical functional hierarchy[7]. Therefore, we investigated how biophysical factors influence the topological organization of FC to determine the underlying factors influencing and shaping functional hierarchy.

To unravel the hierarchical architecture within functional networks, Margulies *et. al.*, 2016 presented a framework based on topological data analysis to determine the components or *gradients* that describe the maximum variance in a network[7]. Briefly, gradient analysis relies on computing the similarity in nodal connectivity patterns followed by dimensionality reduction to extract orthogonal components (gradients) that encode the dominant differences in nodes' connectivity patterns. We leverage their framework to determine how the architecture of the primary gradients of RFNs differ from that of the brain's functional connectivity in order to determine the role biophysical networks have in shaping the hierarchical architecture (see Methods for details).

In **Fig. 6A** we show scatter plots of two primary connectivity gradients for different networks and color them based on the functional communities part of the Schaefer atlas. These primary gradients are the top two topological components to describe the differences in nodal connectivity patterns. For FC_{Full}, we replicate previously presented findings and relative organization of different communities. The observed organization places the default-mode network (DMN), somatomotor (SOM), and visual cortex (VIS) at opposite ends of the spectrum with the Gradient 2 largely separating the DMN from SOM.

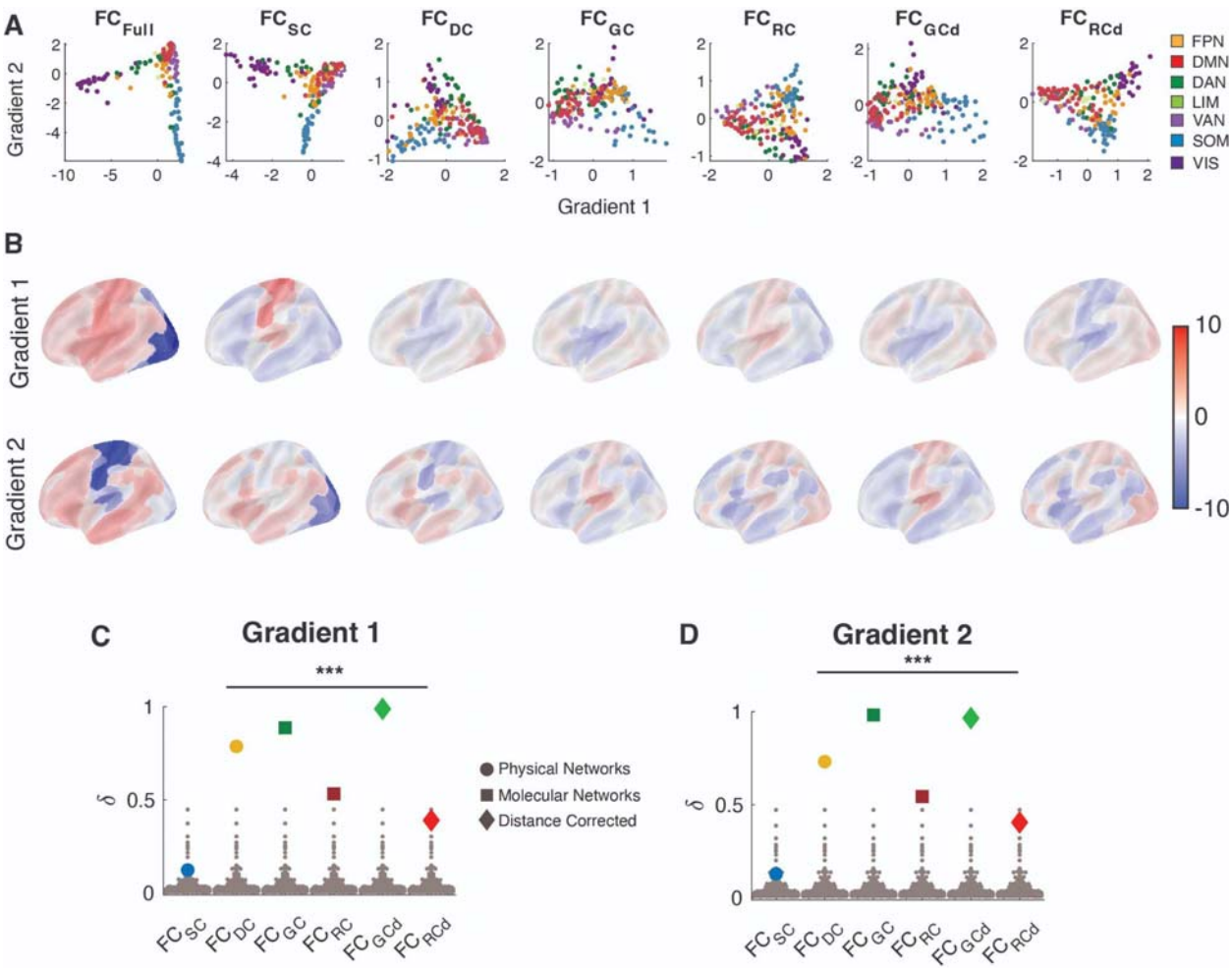

Figure 6. Biophysical networks shape the topological organization of functional brain connectivity. (A) The first two connectivity gradients estimated from the fully connected functional brain network (FC_{Full}), and RFNs, i.e., after removing direct connections associated with SC, DC, GC and RC, GC_d and RC_d. (B) Brain plots of Gradient 1 (*top*) and Gradient 2 (*bottom*). Shift in (C) Gradient 1 and (D) Gradient 2 for different RFNs. Given the complexity of the gradient metric, here to estimate the shift, we calculate the Pearson correlation (R) between the gradient map of FC_{Full} and RFNs and then calculate the shift δ as 1-|R| implying dissimilarity in gradient profiles. The gray dots represent the estimated change – dissimilarity – for the null model which was constructed by removing a set of random connections from the functional connectivity network FC_{Full}. FPN, Frontoparietal Network; DMN, Default Mode Network; DAN, Dorsal Attention Network; LIM, Limbic; VAN, Ventral Attention Network; SOM, Somatomotor; VIS, Visual Network. Statistical testing assessed the deviation from the null model with *** denoting p-value < 0.001.

Removing GC and GC_d connections destroys the relative placement of different communities compared to FC_{Full} whereas the impact of removing SC is relatively low. Removing all other biophysical networks preserves some aspects of the organization (**Fig. 6A, B**). To quantify these

observations, we estimated the shift between FC_{Full} and RFN gradients, δ, by first calculating the Pearson correlation (R) between the gradient map and then calculating δ as 1-|R|, implying dissimilarity in gradient profiles. We also compared the δ estimated from each RFN to a null model in the same manner as was done on the graph-theoretic measures. Reflecting the qualitative observations, GC had the most pronounced effects on both Gradients 1 ($\delta = 0.88$, $P_{rand} < 0.001$; **Fig. 6C**) and Gradient 2 ($\delta = 0.98$, $P_{rand} < 0.001$; **Fig. 6D**). In fact, correcting for distance dependencies in GC increased the effect.

DC also showed a prominent effect on both Gradients 1 ($\delta = 0.78$, $P_{rand} < 0.001$; **Fig. 6C**) and Gradient 2 ($\delta = 0.73$, $P_{rand} < 0.001$; **Fig. 6D**). On the other hand, the effect of RC networks is substantially lower while the effect of SC is below significance level. These observations imply that distance and genetics play a pivotal role in shaping the observed topological organization in FC.

To test the robustness of these results, we tested if the observed differences in RFNs is a function of the percent variance explained by each gradient between different RFNs. As described in **Fig. S2A**, we did not observe any substantial differences in the percent variance explained by each gradient between RFNs, indicating that the observed shifts were not driven by changes in the amount of variance explained between gradients, but can in fact be attributed to different underlying biophysical factors.

A strong dependence of topological gradients on GC indicates that topological organization could reflect genetic relationships between brain regions. However, the prominence of DC suggests that confounds such as spatial auto-correlations may also drive overall topological organization of the functional connectivity. Therefore, caution is warranted when attributing topological organization solely to hierarchical cognitive architecture. Nonetheless, unlike graph-theoretical measures, which were completely dominated by molecular factors, we see a substantial influence of a physical factor when higher-order interactions are considered.

<u>Robustness of the relationship between biophysical networks and FC</u>

The analysis on graph-theoretic and topological organization was based on the magnitude (i.e. |correlation|) of the FC. To test that this choice did not affect our results, we conducted an additional analysis where we first thresholded the FC at zero to remove all negative connections[17,18]. We observed differences in the magnitude of network features, as expected, however, we observed a clear dominance of the effect of molecular factors on graph-theoretical features replicating our main findings (**Fig. S3B**). Similarly, we observed a prominent effect of DC on topological gradients (**Fig. S3C-D**). The effect of molecular factors was somewhat nuanced; GC showed a dominant effect on Gradient 2, as discussed in Fig. 6, but Gradient 1 had a higher impact of RC as compared to both GC and DC.

Moreover, we examined the robustness using a different null-model where instead of removing connections from FC_{Full} at random, we generated multiple randomized biophysical networks by re-wiring a given biophysical network and removing these randomized networks from FC_{Full}. Specifically, the connections in each biophysical network were randomized while preserving the degree distribution[19]. As discussed in **Fig. S4**, we obtained similar results for the re-wired null model for both graph-theoretic and topological properties replicating all our main findings discussed in Figures 4 and 6.

Additionally, we corroborated our main findings using additional resting-state fMRI data recorded from 130 healthy individuals from the LA5c dataset[13]. The goal of the LA5c dataset was to understand the dimensional structure of memory and cognitive control in both healthy individuals and individuals with neuropsychiatric disorders including schizophrenia, bipolar disorder, and attention deficit/hyperactivity disorder. For the corroborative analysis, we utilized approximately 5 minutes of resting-state fMRI data in the healthy population and the results are described in **Figs. S5 and S6**.

Similar to our findings in HCP (**Fig. 3**) biophysical networks exerted the strongest effects on the modularity (Δ = 39.67 ± 16.45%; **Fig. S5A**). Moreover, FC was most strongly constrained and shaped by molecular factors (GC: Δ = 20.52 ± 15.73% and RC: Δ = 19.41 ± 18.86%) reflecting the findings in the HCP dataset (**Fig. S5B-I**). While molecular factors dominate in both HCP and LA5c, we observed a relatively higher impact of genetic similarity between brain regions (GC)

in LA5c than in the HCP dataset in which RC was the dominant molecular factor. However, as was found in the HCP dataset, SC had the least effect on FC organization. Further, the findings from the topological analysis revealed a dominance of DC and GC on topological Gradient 2, and DC on topological Gradient 1 (**Fig. S6B-C**), similar to the findings discussed in **Fig. 6**. However, we found a more nuanced effect of molecular factors on topological Gradient 1. Additionally, we observed a significant effect of SC on topological gradients, unlike what was observed in HCP data.

Across these various robustness tests, we observed a clear dominance of molecular factors on the graph-theoretical organization of functional connectivity. Some of the topological features showed variations across the datasets, but the dominant effect of DC was robustly observed on the topological organization of functional connectivity for different methodological and data choices considered in this study.

<u>Predicting FC from underlying biophysical networks</u>

The above analysis indicates that molecular factors constrain and shape the pairwise relationships between brain regions. Therefore, as an additional analysis to establish the robustness of our findings, we determined how well each of the biophysical networks could predict FC. We observed that the biophysical networks exhibited differential capabilities when predicting FC (**Fig. S7**). On average the best predictor of nodewise functional connectivity was neuroreceptor congruence ($R^2 = 0.31 \pm 0.16$; $P < 0.001$). Whereas the other biophysical networks exhibited weak or localized predictive capabilities. Moreover, neuroreceptor congruence was the best predictor of functional connectivity in the healthy control group from the LA5c dataset, reflecting the results in the HCP dataset (**Fig. S8**). Together these results confirm the dominance of molecular factors in constraining and shaping functional connectivity across the cortex.

<u>Biophysical networks underlie neuropsychiatric induced changes in FC</u>

Lastly, we investigated if specific biophysical networks underlie the changes in functional connectivity observed in neuropsychiatric populations. The deviations in the case of neuropsychiatric conditions tend to be more nuanced[20,21]. We aimed to uncover if these changes can be attributed to different biophysical factors to a varied extent. We leveraged the LA5c

dataset which also included individuals with neuropsychiatric disorders – schizophrenia (N=50), attention deficit/hyperactivity disorder (N=40), and bipolar disorder (N=37)[13]. The strength of the LA5c dataset is that it allowed us to include a diverse set of neuropsychiatric disorders while minimizing the issues related to experimental protocol and measurement differences.

First, we tested if the functional connectivity tends to increase or decrease in the above clinical groups. We performed an edgewise independent sample t-test to identify connections that changed due to schizophrenia (SCZ), attention deficit/hyperactivity disorder (ADHD) and bipolar disorder (BD) compared to healthy individuals, respectively. We observed that some connections increased (red) and others decreased (blue) in strength compared to healthy individuals (**Fig. 7**) with overall functional connectivity increasing in SCZ (average t-value = 0.30 ± 0.009; **Fig. 7A**) and decreasing in ADHD (average t-value = -0.35 ± 0.007; **Fig. 7C**) and BD (average t-value = -0.47 ± 0.007; **Fig. 7E**). We then investigated whether these alterations were shaped significantly by specific biophysical networks.

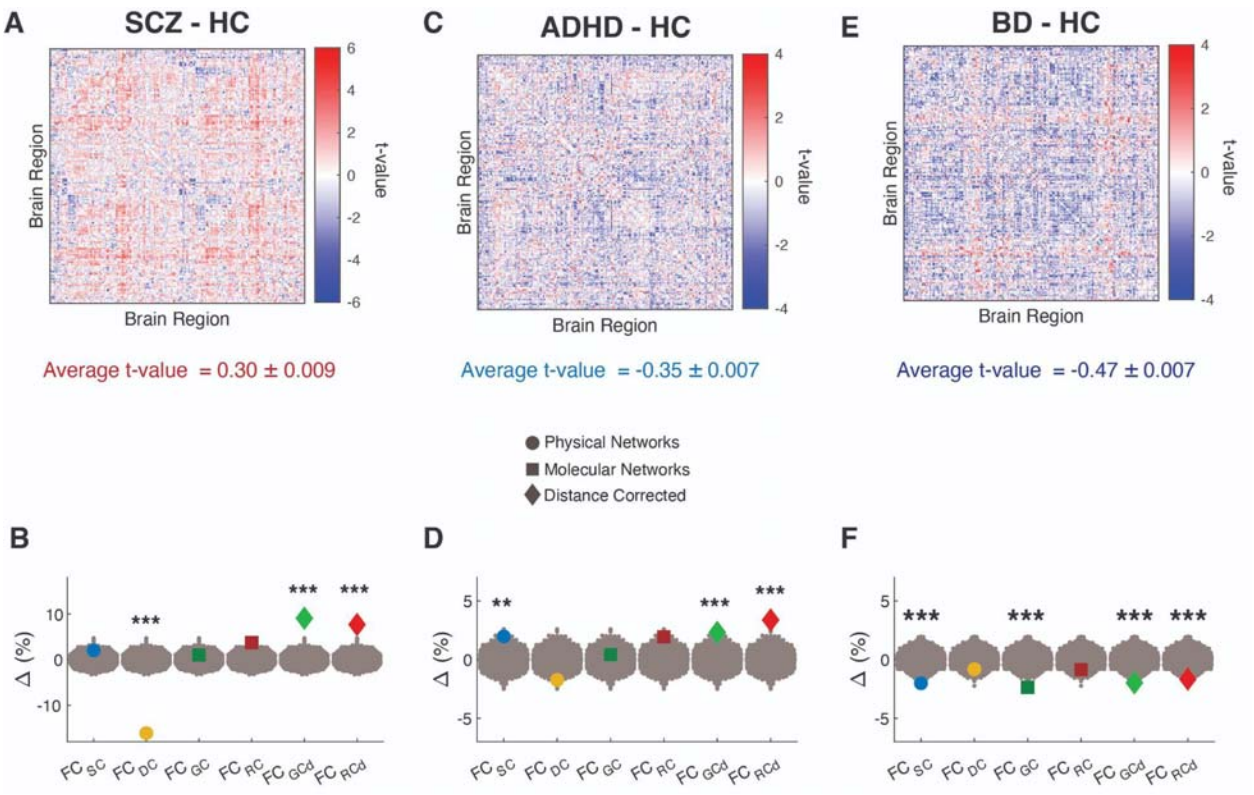

Figure 7. Neuropsychiatric disorders induced changes in functional connectivity are related to biophysical networks. (A) Differences in functional connectivity (independent samples t-tests) between schizophrenia (SCZ) and healthy controls (HC) with average t-value shown at the bottom. (B) Biophysical networks induced percent change in average t-value. We constructed RFNs from the t-value matrix by removing connections specific to each biophysical network and computed the shift Δ as a percent change in average t-value. (C, D) Same as panel A and B respectively, but for attention deficit/hyperactivity disorder (ADHD). (E, F) Same as panel A and B respectively, but for bipolar disorder (BD). Statistical testing assessed observed differences in RFNs compared to a null model (gray dots) based on removing an equal number of random connections with *** denoting p-value < 0.001.

Next, to determine how biophysical networks impacted observed changes in the functional connectivity due to the neuropsychiatric populations, we calculated RFNs from the t-value matrix by removing connections associated with each biophysical network in the same manner as described in Figure 1 and quantified the deviation (Δ) as a percent change in average t-value. A positive Δ indicates that connections associated with a specific biophysical network acted to decrease average FC (i.e negative t-values) in the clinical population as compared to healthy controls and upon removal, the average t-value increased in the corresponding RFN. Similarly, a negative Δ indicates that connections associated with a specific biophysical network acted to

increase average FC in the clinical population. Moreover, we compared the observed changes to a null distribution based on removing an equal number of random connections in the same manner as was conducted for the above analyses.

For schizophrenia, removing spatially auto-correlated connections (DC) resulted in significant decrease in Δ (i.e., -16.10%, $P_{rand} < 0.001$) indicating that DC associated connections were heightened in strength in the schizophrenia group compared to healthy controls (**Fig. 7B**). We did not observe a significant effect of removing SC and molecular factors, i.e., GC and RC ($P_{rand} > 0.05$), whereas, removing the molecular connections corrected for distance, i.e., GC_d (Δ = 9.07%), RC_d (Δ = 7.68%), resulted in significant increase in Δ ($P_{rand} < 0.001$) indicating that these networks dampened functional connectivity in SCZ.

In ADHD, we observed a similar positive effect of distance corrected molecular networks, i.e., GC_d (Δ = 2.32%; $P_{rand} < 0.001$) and RC_d (Δ = 3.38%; $P_{rand} < 0.001$), indicating that these networks dampened functional connectivity, however we found this effect to be much smaller than in case of SCZ (lower Δ values). Similar to SCZ, in ADHD too we did not observe a significant effect of GC and RC, however, unlike in SCZ, SC showed a low but significant positive effect (Δ = 1.97%; $P_{rand} < 0.001$), indicating that SC related connections are dampened in functional connectivity in the ADHD group. We did not observe a significant effect of DC for the ADHD group.

In the BD group we also observed a significant but opposite effect of SC (Δ = -2.00%; $P_{rand} < 0.001$), indicating that SC related functional connections were higher in this clinical group as compared to healthy controls. We also observed a significant negative effect of genetic similarity in both GC (Δ = -2.35%; $P < 0.001$) and GC_d (Δ = -1.97%; $P_{rand} < 0.001$) indicating that connections associated with genetic similarity were heightened in the BD group as well. Additionally, RC_d also led to significant negative change (Δ = -1.66%; $P_{rand} < 0.001$) while DC associated connections did not have a significant effect ($P_{rand} > 0.05$).

Our framework reveals interesting dependencies of the observed alterations in functional connectivity on underlying biophysical networks. We observed that SCZ and ADHD exhibited a

similar relationship between molecular and distance corrected factors and functional connectivity. However, their relationship with physical factors, both SC and DC, differentiated these groups; SCZ is characterized by a strong negative shift due to DC and ADHD is characterized by a positive shift due to SC. On the other hand, BD exhibited a different profile of shifts from SCZ and ADHD across all biophysical networks, with SC and GC driven negative shifts uniquely separating it from the other groups. Overall, we found the effect of molecular factors to be more nuanced across all the groups and a strong dominance of physical factors in differentiating groups.

Discussion

Functional brain connectivity is the cornerstone of cognition, with alterations potentially serving as indicators of pathological states[22]. This large-scale property of the brain, which also provides a window into brain-wide communication, is anchored by various underlying biophysical networks. Here we addressed how various biological factors, physical and molecular, shape the fundamental organizational features of the brain's functional connectivity (FC). Specifically, we considered structural connectivity[8], spatial auto-correlation[9], gene expression similarity[10], and neuroreceptor congruence [11] across regions and dissociated their individual contribution to pairwise (graph-theoretic) as well as higher-order (topological) emergent properties of functional connectivity. We developed a computational framework leveraging remnant functional networks to determine the contribution of biophysical networks in shaping functional connectivity and further assess how these factors drive the functional connectivity alterations observed in groups with neuropsychiatric disorders.

In order to fully unravel the role of biophysical networks, we leveraged a comprehensive set of quantitative features derived from graph theory and topology, two branches of mathematics that have been instrumental in understanding the foundational features in the complex neuroimaging data[23]. With the help of these features, we quantified and compared the organization of functional connectivity networks and remnant functional networks that were constructed from functional connectivity after removing connections associated with a given biophysical network. Our findings robustly indicate that molecular factors, i.e., neuroreceptor congruence and

similarity in gene expression between regions play a prominent role in shaping the graph-theoretic organization of the resting-state functional brain connectivity estimated with fMRI.

In particular, neuroreceptor congruence among brain regions stood out as the robust dominant factor shaping a wide spectrum of graph-theoretical properties that have been discussed to capture a variety of functions in the brain including efficient processing of information[4], robustness to malfunction[6] and global excitation[24], and even the emergence and termination of seizures[25]. In general, we observed a higher shift in graph-theoretical features, such as weighted degree and clustering coefficient, after removing molecular factors, and we found a unique relationship between the magnitude of the shift with both weighted degree and clustering coefficient for neuroreceptor congruence (Fig. 5 and Fig. S1) implying its prominent role in shaping hub-like regions in the brain which underlie efficient integration and segregation of information[5]. Additionally, using search information-based modeling (Fig. S7 and S8) we found that the neuroreceptor congruence was the best predictor of functional connectivity[26]. This reliance on neuroreceptor congruence could suggest that pairwise interactions in functional brain connectivity emerge more substantially from a similar response to neurotransmitters across the brain than any other factor considered in this study.

Differing from graph-theoretic features, we found a mix of physical and molecular factors, more robustly spatial auto-correlation and similarity in gene expression, to shape the topological features of functional connectivity capturing higher-order interactions. The shared genetic profiles may provide a foundation for the topological organization that is linked to the functional specialization or hierarchy observed in the brain networks[7]. However, the strong and robust dependence on spatial auto-correlation we observed across different methodological choices and datasets may suggest a more physical basis of topological organization. These results also reflect previous findings of Watson *et. al.,* 2023 showing that gradients identified by connectopic mapping techniques reflect confounds associated with spatial auto-correlations[27]. Irrespective of the overall interpretation of the topological organization, our analysis robustly establishes the role of spatial auto-correlation in driving the higher-order interactions in the functional brain connectivity.

Surprisingly, our results suggest that structural connections provide a limited understanding to the biophysical underpinnings of the brain's functional connectivity. Structural pathways are undoubtedly critical for facilitating communication between neurons and maintaining healthy brain states[28], but our study highlights the limitations when inferring functional connectivity directly from structural connections estimated with diffusion MRI[29]. Factors such as the composition of the neuroreceptors on dendrites can amplify signals from weak structural connections or diminish signals from strong connections, thus making it difficult to infer the extent of functional connectivity from structural connections alone[30]. These findings suggest that for a more holistic understanding of how functional connectivity arises, we need to refine the modeling frameworks that largely rely on structural connectivity, and we need to better understand how genetic expression and neuroreceptor congruence across the cortex shapes brain-wide communication.

Further, using our framework we determined the factors that are the major source of the alterations in functional connectivity due to neuropsychiatric disorders. Consistently in schizophrenia, bipolar disorder, and ADHD, a complex interaction between biophysical networks underly the observed changes in functional connectivity. However, we observed a clear dominance of physical factors in differentiating disorder specific alterations. In particular, we observed a very strong impact of spatial auto-correlation uniquely in schizophrenia indicating that connections associated with distance dependent connectivity were heightened. Whereas, structural connectivity driven differences separated all the groups, such that SC related functional connections were enhanced in bipolar disorder, unaffected in SCZ, and dampened in ADHD as compared to healthy controls. Further studies are necessary to validate these findings in bigger datasets as well as to assess regional specificity in connectivity alterations. Nonetheless, our analysis provides specific targets and hypotheses to develop and test disease specific diagnosis and perhaps treatment.

Some considerations are warranted while interpreting our findings and designing follow up analysis. Importantly, the focus of the analysis has been on understanding the relationship between biophysical networks and functional connectivity at the macroscale, but it remains unknown whether the relationships observed here are reflected at a more microscopic scale of

neurons and neural circuits. Additionally, our analysis focused on four distinct types of biophysical networks, but biophysical networks can be estimated from a multitude of other factors such as similarity in neuronal composition[31] or cytoarchitecture[32] between brain regions which might also impact the organization of functional connectivity. Nonetheless, our framework provides a means to assess the relationship between functional connectivity and multiple biophysical networks ranging from the micro (i.e. neurons) to the macroscale.

In conclusion, our study highlights that biophysical factors, both physical and molecular, play a role in shaping the fundamental emergent properties of the brain's functional connectivity. These factors should be accounted for while creating working models of functional connectivity and sole reliance on the structural connectivity should be avoided. However, the contributions of different biophysical factors are not equitable, and these factors differentially shape distinct aspects of functional connectivity. Molecular factors, particularly neuroreceptor congruence, dominantly shape graph-theoretic properties that capture pairwise interactions in functional connectivity, while a mix of molecular and physical factors, particularly, spatial auto-correlation and similarity in gene expression drive the topological organization of functional connectivity capturing higher-order interactions. Additionally, physical factors, including spatial auto-correlation and structural connectivity seem to better differentiate disease specific alterations. These findings can be factored in to understand and model functional connectivity in various specific applications. While our present study focuses on the resting-state functional connectivity, our analysis provides a simple yet powerful test to further examine how various underlying factors uniquely and/or dynamically shape functional connectivity in varied domains including during task performance, development, and clinical.

Methods

Analytical framework

Remnant functional networks (RFNs)

We propose remnant functional networks (RFNs) to quantify the contribution of underlying biophysical networks in shaping functional brain connectivity. The critical idea behind the framework is that it quantifies and compares the change in the organization of functional networks when shared connections between the functional brain network and a biophysical network of interest, i.e., structural connectivity, spatial auto-correlation, similarity in gene expression, or neuroreceptor congruence, are removed (**Fig. 1**).

Specifically, first we estimate the functional connectivity between brain regions using the BOLD signal from functional MRI. This results in a fully connected weighted functional network (FC_{Full}; **Fig. 1A**). Second, connections in FC_{Full} that also have a corresponding connection in the reference biophysical network (e.g., SC, DC, GC or RC) are removed (**Fig. 1B)**. For instance, when the reference network is SC, procedurally this entails setting all connections in the FC_{Full} network to zero that also have structural connections; this produces a weighted functional network with connections remnant to (indirect) structural connections (FC_{SC}; **Fig, 1C**; note that the subscript corresponds to the connections that are removed). The same procedure is repeated for DC, GC and RC based networks resulting in weighted networks with only remnant connections, i.e., FC_{DC}, FC_{GC}, FC_{RC}, respectively.

Quantifying the shifts in RFN

Critically, to determine which features of the functional network SC, DC, GC and RC shape, we quantify the magnitude of the change in the feature after removing SC, DC, GC or RC from the functional network. Specifically, a feature (e.g., network modularity) of the network is estimated in FC_{Full} which we label as P_{Full}. Then, the same feature is calculated for RFNs, i.e., $FC_{SC,}$ FC_{DC}, FC_{GC}, FC_{RC} networks, and for simplicity we label these as P_{SC}, P_{DC}, P_{GC}, and P_{RC}. Further, to assess the statistical significance, we constructed a null model by removing an equal number of connections from the functional connectivity at random (details below). We iterated on this process 1000 times and generated a null distribution.

Functional MRI Data

HCP Resting-State Functional Connectivity

We used pre-processed resting-state functional MRI (fMRI) data from 48 healthy human subjects from the Human Connectome Project (HCP)[12]. (Note we downloaded 50 subjects, but two were missing data). In brief, subjects underwent four sessions of 15-min resting-state scanning sessions. fMRI volumes were recorded using a customized 3T Siemens Connectome Skyra scanner with an EPI sequence (TR = 0.72 s, TE = 33.1 ms, 72 slices, 2.0 mm isotropic, field of view (FOV) = 208 × 180 mm). In addition to the pre-processing steps part of the HCP pipeline, we additionally regressed out the global signal. The data was mapped on Schaefer atlas to derive 200 ROIs (brain regions)[14]. The same atlas was used in all subsequent biophysical networks as well (see below).

UCLA Consortium for Neuropsychiatric Phenomics Dataset (LA5c)

The Consortium for Neuropsychiatric Phenomics includes imaging of healthy individuals (N=122), individuals diagnosed with schizophrenia (N=50), bipolar disorder (N=37), and attention deficit hyperactivity disorder (N=40)[13]. In brief, resting-state functional MRI scan were obtained while subjects kept their eyes open for 304 s in the scanner. Neuroimaging data were acquired on a 3T Siemens Trio scanner. T1-weighted high-resolution anatomical scans (MPRAGE) were collected with a slice thickness = 1mm, 176 slices, TR=1.9s, TE=2.26ms, matrix=256 x 256, FOV=250mm. Resting-state MRI data were collected with a T2*-weighted EPI sequence with slice thickness = 4mm, 34 slices, TR=2s, TE=30ms, flip angle=90°, matrix=64 × 64, FOV=192mm.

The analysis was based on minimally preprocessed data using FMRIPREP version 0.4.4 (http://fmriprep.readthedocs.io). T1 weighted volume was corrected for bias field using ANTs N4BiasFieldCorrection v2.1.0 skullstripped and coregistered ICBM 152 Nonlinear Asymmetrical template. Resting-state data were motion corrected using MCFLIRT v5.0.9. Functional data was skullstripped and coregistered to the corresponding T1 weighted volume using boundary-based registration. Motion correcting transformations, transformation to T1 weighted space and MNI template warp were applied in a single step using antsApplyTransformations. Framewise displacement and Dvars were calculated using Nipype

implementation. In addition to those regressors, global signal and mean white matter signal was also calculated and removed.

Functional connectivity networks

For each individual, to extract functional connectivity we computed the magnitude of correlation in BOLD activity from a pair of regions across 200 regions derived from the Schaefer Atlas[14]. For the HCP analysis a group functional connectivity network was estimated by averaging the individual subject networks together. The replication analysis using the LA5c dataset, a similar group functional connectivity network was estimated by averaging the individual subject networks together. The main analyses on the HCP dataset were based on the magnitude of the functional connections. We additionally replicated the findings in FC networks thresholded at zero in the HCP. Moreover, replication on the LA5c dataset was based on the magnitude of the functional connections.

Biophysical networks

Diffusion MRI based structural connectivity (SC)

Preprocessed diffusion weighted images for each of the 48 subjects part of the HCP S1200 release were used to construct structural connectomes. Specifically, fiber tracking was done using DSI Studio with a modified FACT algorithm[33]. Data were reconstructed using generalized q-sampling imaging (GQI) in MNI space. Fiber tracking was performed until 250,000 streamlines were reconstructed with default parameters. For each subject, an undirected weighted structural connectivity matrix, A, was constructed from the connection strength based on the number of streamlines connecting two regions. Connectivity matrix was normalized by dividing the number of streamlines (T) between region *i* and *j*, by the combined volumes (*v*) of region *i* and *j*.

$$A_{ij} = \frac{T_{ij}}{v_i + v_j}$$

Group structural connectivity was estimated by averaging all the individual structural connectivity networks together. The group structural connectivity network was then thresholded to match the average density across individual subjects.

Spatial auto-correlation or distance derived connectivity (DC)

Functional connectivity between brain regions has been shown to be dependent on the physical proximity between regions, spatial auto-correlation. The distance between two regions was estimated as the Euclidean Distance (D) between their centroids. Since brain regions that are farther apart are going to have larger values, the matrix was converted to a proximity matrix (DC) by subtracting each entry from the largest value in the matrix as follow:

$$DC = D_{max} - D$$

Where D_{max} represents the value associated with the farthest brain regions.

Genetic expression-based connectivity (GC)

Genetic expression dependent connectivity aims to estimate the extent of the similarity in genetic expression profiles between brain regions and relate the similarity in genetic expression to functional connectivity. Regional microarry expression data were obtained from 6 post-mortem brains (1 female, ages 24.0--57.0, 42.50 +/- 13.38) provided by the Allen Human Brain Atlas (AHBA, https://human.brain-map.org)[15]. Data was processed with the abagen toolbox (version 0.1.3; https://github.com/rmarkello/abagen).

Microarray probes were reannotated using data provided by Arnatkevic□iūtė *et. al.*, 2019[34]; probes not matched to a valid Entrez ID were discarded. Next, probes were filtered based on their expression intensity relative to background noise[35], such that probes with intensity less than the background in >=50.00% of samples across donors were discarded , yielding 31,569 probes . When multiple probes indexed the expression of the same gene, we selected and used the probe with the most consistent pattern of regional variation across donors (i.e., differential stability[36]), calculated with:

$$\Delta_s(p) = \frac{1}{\left(\frac{N}{2}\right)} \sum_{i=1}^{N-1} \sum_{j=i+1}^{N} \rho\,[B_i(p), B_j(p)]$$

Where ρ is Spearman's rank correlation of the expression of a single probe, p, across regions in two donors B_i and B_j, and N is the total number of donors. Here, regions correspond to the structural designations provided in the ontology from the AHBA.

The MNI coordinates of tissue samples were updated to those generated via non-linear registration using the Advanced Normalization Tools (ANTs; https://github.com/chrisfilo/alleninf). To increase spatial coverage, tissue samples were mirrored bilaterally across the left and right hemispheres. Samples were assigned to brain regions in the provided atlas if their MNI coordinates were within 2 mm of a given parcel. All tissue samples not assigned to a brain region in the provided atlas were discarded.

Inter-subject variation was addressed by normalizing tissue sample expression values across genes using a robust sigmoid function[37]:

$$x_{norm} = \frac{1}{1 + exp(-\frac{(x - < x >)}{IQR_Z})}$$

where $< x >$ is the median and IQR_z is the normalized interquartile range of the expression of a single tissue sample across genes. Normalized expression values were then rescaled to the unit interval:

$$x_{scaled} = \frac{x_{norm} - min(x_{norm})}{max(x_{norm}) - min(x_{nomr})}$$

Gene expression values were then normalized across tissue samples using an identical procedure. Samples assigned to the same brain region were averaged separately for each donor and then across donors, yielding a regional expression matrix with 200 rows, corresponding to brain regions, and 15,633 columns, corresponding to the retained genes. Similarity in genetic expression (GC) between brain regions was estimated using the Pearson correlation.

Neuroreceptor congruence-based connectivity (RC)

Neuroreceptor dependent connectivity aims to estimate the extent of the similarity in neuroreceptor profiles between brain regions and relate the similarity in neuroreceptor

congruence to functional connectivity. The analysis used data originally published in Hansen et al.,[11]. In brief, PET tracer imaging was used to map the density for 19 neuroreceptors and transporters. The neuroreceptors include 9 neurotransmitter systems: dopamine (D_1, D_2, DAT), norepinephrine (NET), serotonin (5-HT_{1A}, 5-HT_{1B}, 5-HT_{2A}, 5-HT_4, 5-HT_6, 5-HTT), acetylcholine ($\alpha 4\beta 2$, M1, VAChT), glutamate ($mGluR_5$, NMDA), Gamma-aminobutyric acid ($GABA_A$), histamine (H3), cannabinoid (CB1), and μ-opioid neuroreceptor (MOR). Each PET tracer image was parcellated onto 200 cortical regions and z-scored. A neuroreceptor similarity (RC) matrix was constructed using the Pearson correlation between the neuroreceptor profiles among the 200 cortical regions.

Distance Correction

Since the similarity in gene expression and neuroreceptor composition between two regions can be dependent on the distance, we created two additional networks that controlled for distance. We regressed the similarity due to spatial auto-correlation from the GC and RC networks to generate a distance controlled genetic network – GC_{ED} – and neuroreceptor network – RC_{ED}.

Density matching

The DC, GC, GC_{ED}, RC and RC_{ED} are fully connected networks compared to the SC network, which is sparsely connected, therefore, density matching was required to be able to compare the effect of removing each of these networks. We thresholded these networks to match the density of the SC network. As a result, the most prominent connections survived in the biophysical networks.

Graph-theoretical properties

We used multiple network properties to capture distinct aspects of the organization of functional brain connectivity. All properties were estimated using the Brain Connectivity Toolbox[38]. The specific properties measured are:

Weighted Degree

The weighted degree (k_i) is defined as the sum of all connections for a brain region

$$k_i = \sum_{j \in N} W_{ij}$$

where W is the weighted adjacency matrix of a network with N number of brain regions[38]. The degree of nodes is an indicator of how important a node is for communication between brain regions[38].

Clustering Coefficient

The weighted clustering coefficient (CC) for a brain region i is the intensity of triangles in a network calculated as,

$$CC_i = \frac{1}{b_i\,(b_1 - 1)} \sum_{j,h} (w_{ij}\, w_{ih}\, w_{jh})^{1/3}$$

where w is the weighted adjacency matrix and b is the number of connections for brain region i and assess the extent of segregation in a network[38].

Eigenvector Centrality

Eigenvector centrality (EC_i) measures how influential a brain region is in a network, with a high value indicating a brain region is connected to other highly influential regions[39,40]. The eigenvector centrality of a brain region i is given by the i-th entry in the dominant eigenvector, which is the vector $\boldsymbol{v}=[v_1,\ldots v_N]$ that solves

$$\lambda_1 v = W v^T$$

where λ_1 is the largest eigenvalue of the weighted adjacency matrix, W.

Modularity

Modularity (Q) quantifies the extent to which the brain functional connectivity may be subdivided into modules[38]. Specifically, for a given network W, Q is estimated as:

$$Q = \Sigma_{ij}\, [W_{ij} - \gamma P_{ij}]\delta(c_i, c_j)$$

where P_{ij} is the expected partition from a null model; γ is the resolution parameter ($\gamma = 1$); c_i and c_j represent the module assigned to brain region i and j are; $\delta(c_i,c_j)$ is the Kronecker delta function and is equal to one when $c_i = c_j$, and is zero otherwise. Modules are thought to be a key element for cognition in which discrete processes occur[41].

Path Length

The characteristic path length (L) is the average shortest path length between all brain regions[38],

$$L = \frac{1}{N}\sum_{\in N}\frac{\sum_{j\in N, j\neq i} \mathrm{d}_{ij}^{w}}{N-1}$$

where is the distance between brain region i and j. To calculate, we first take the inverse of the edge weights to transform the weight to a measure of length (i.e., to transform a strong connection strength to a short length). The brain organization has been shown to be shaped by an economic trade-off between minimizing costs and allowing distant regions to communicate efficiently in order to adapt to changing environmental demands[42].

Spectral Radius

The spectral radius measures the ease with which diffusion process can occur in a network. The spectral radius is calculated as,

$$\rho(w) = max\{|\lambda_1|, \ldots, |\lambda_n|\}$$

where $|\lambda|$ corresponds to the absolute value of the eigenvalues of a network. Spectral radius reflects the excitability of brain networks[24,25].

Synchronizability

Synchronizability is a measure of linear stability for a network of coupled dynamical systems[43],

$$S = \frac{\lambda_2}{\lambda_n}$$

where λ_2 is the second smallest eigenvalue of the unnormalized Laplacian matrix (L) and λ_n is its largest eigenvalue. The Laplacian is calculated as,

$$L = K - W$$

where K is the degree matrix of the functional connectivity matrix, W. Synchronizability assesses the ability of distant brain regions to synchronize[44].

<u>Topological organization (cortical gradients)</u>

The hierarchical organization of functional brain connectivity is estimated using the framework based on topological gradients of Margulies *et. al*,[7]. Topological gradients were estimated with the BrainSpace Toolbox[45]. Specifically, FC_{Full} and RFNs were thresholded so that top 10% of connections were maintained and cosine similarity was used to estimate the similarity in the

connectivity profiles between brain regions within each network, respectively. Analysis was based on the first two gradients identified using diffusion maps. All RFNs gradients were aligned to the FC_{Full} gradients using procrustes alignment.

Search information based modeling

Search information (SI) was used to model functional connectivity between brain regions. SI measures the amount of information (in bits) required to traverse the shortest paths between a given pair of nodes[26]. The resulting SI matrix can be considered a proxy for the extent of functional connectivity between brain regions. Specifically, an SI matrix was estimated from each of the biophysical networks and the SI profile of each brain region was compared to the empirical functional connectivity profile[46]. Note that higher (lower) SI values imply lower (higher) functional connectivity. In order to equate the relationship, the SI values were reversed by

$$SI = SI_{max} - SI$$

Where SI_{max} represents the value associated with the farthest brain regions.

Null Models

Null model was used to benchmark the effects of removing SC, DC, GC and RC associated connections in the FC. Specifically, if a specific network feature in the FC is dependent on an underlying network, then the change in that feature after removing SC, DC, GC or RC associated connections should result in a change that is larger than what would be found with removing a random set of connections. To determine this, we used two different null models – random connections and re-rewired.

Random Connections

RFN null model was estimated by removing a random set of connections from the FC network that matched the number of connections in the biophysical network and the change in the network feature was calculated. This process was repeated 1,000 times to generate a null distribution for that feature.

Re-wired Null Model

To test the robustness of our results we used another null model that was estimated by removing a re-wired set of connections that preserved the degree of each node in the biophysical networks. This process was repeated 1,000 times to generate a null distribution for that feature. The re-rewired null model was generated using the Brain Connectivity Toolbox[38].

Data Availability

Minimally pre-processed Human Connectome Project data can be downloaded from https://www.humanconnectome.org/. Genetic expression data can be obtained using the abagen toolbox (https://abagen.readthedocs.io/en/stable/installation.html). Neuroreceptor composition data can be obtained at https://github.com/netneurolab/hansen_receptors. The brain connectivity toolbox can be downloaded at https://sites.google.com/site/bctnet/. Brainspace toolbox can be downloaded at https://brainspace.readthedocs.io/en/latest/pages/install.html.

References

1. Bassett, D. S. & Sporns, O. Network neuroscience. *Nature neuroscience* **20**, 353–364 (2017).
2. Chadick, J. Z. & Gazzaley, A. Differential coupling of visual cortex with default or frontal-parietal network based on goals. *Nature Neuroscience* **14**, 830–832 (2011).
3. Cole, M. W., Ito, T., Bassett, D. S. & Schultz, D. H. Activity flow over resting-state networks shapes cognitive task activations. *Nature Neuroscience* (2016) doi:10.1038/nn.4406.
4. Avena-Koenigsberger, A., Misic, B. & Sporns, O. Communication dynamics in complex brain networks. *Nature Reviews Neuroscience* **19**, 17–33 (2017).
5. Cohen, J. R. & D'Esposito, M. The Segregation and Integration of Distinct Brain Networks and Their Relationship to Cognition. *J. Neurosci.* **36**, 12083 (2016).
6. Aerts, H., Fias, W., Caeyenberghs, K. & Marinazzo, D. Brain networks under attack: Robustness properties and the impact of lesions. *Brain* **139**, 3063–3083 (2016).
7. Margulies, D. S. *et al.* Situating the default-mode network along a principal gradient of macroscale cortical organization. *Proceedings of the National Academy of Sciences* **113**, 12574–12579 (2016).
8. Honey, C. J. *et al.* Predicting human resting-state functional connectivity from structural connectivity. *Proceedings of the National Academy of Sciences* (2009) doi:10.1073/pnas.0811168106.
9. Shinn, M. *et al.* Functional brain networks reflect spatial and temporal autocorrelation. *Nature Neuroscience* **26**, 867–878 (2023).
10. Richiardi, J. *et al.* Correlated gene expression supports synchronous activity in brain networks. *Science* **348**, 1241–1244 (2015).
11. Hansen, J. Y. *et al.* Mapping neurotransmitter systems to the structural and functional organization of the human neocortex. *Nature Neuroscience* **25**, 1569–1581 (2022).
12. Van Essen, D. C. *et al.* The WU-Minn Human Connectome Project: An overview. *NeuroImage* (2013) doi:10.1016/j.neuroimage.2013.05.041.
13. Poldrack, R. A. *et al.* A phenome-wide examination of neural and cognitive function. *Scientific Data* **3**, 160110 (2016).
14. Schaefer, A. *et al.* Local-Global Parcellation of the Human Cerebral Cortex from Intrinsic Functional Connectivity MRI. *Cerebral Cortex* **28**, 3095–3114 (2018).
15. Hawrylycz, M. J. *et al.* An anatomically comprehensive atlas of the adult human brain transcriptome. *Nature* **489**, 391–399 (2012).
16. Medaglia, J. D., Lynall, M.-E. & Bassett, D. S. Cognitive Network Neuroscience. *Journal of Cognitive Neuroscience* **27**, 1471–1491 (2015).
17. Zhan, L. *et al.* The significance of negative correlations in brain connectivity. *Journal of Comparative Neurology* **525**, 3251–3265 (2017).
18. Schwarz, A. J. & McGonigle, J. Negative edges and soft thresholding in complex network analysis of resting state functional connectivity data. *NeuroImage* **55**, 1132–1146 (2011).
19. Maslov, S. & Sneppen, K. Specificity and Stability in Topology of Protein Networks. *Science* **296**, 910–913 (2002).
20. Winter, N. R. *et al.* Quantifying Deviations of Brain Structure and Function in Major Depressive Disorder Across Neuroimaging Modalities. *JAMA Psychiatry* **79**, 879–888 (2022).
21. Segal, A. *et al.* Regional, circuit and network heterogeneity of brain abnormalities in psychiatric disorders. *Nature Neuroscience* **26**, 1613–1629 (2023).

22. Fornito, A., Zalesky, A. & Breakspear, M. The connectomics of brain disorders. *Nature Reviews Neuroscience* **16**, 159–172 (2015).
23. Centeno, E. G. Z., Moreni, G., Vriend, C., Douw, L. & Santos, F. A. N. A hands-on tutorial on network and topological neuroscience. *Brain Structure and Function* **227**, 741–762 (2022).
24. Bansal, K., Medaglia, J. D., Bassett, D. S., Vettel, J. M. & Muldoon, S. F. Data-driven brain network models differentiate variability across language tasks. *PLoS Computational Biology* (2018) doi:10.1371/journal.pcbi.1006487.
25. Rungratsameetaweemana, N. *et al.* Brain network dynamics codify heterogeneity in seizure evolution. *Brain Communications* **4**, fcac234 (2022).
26. Goni, J. *et al.* Resting-brain functional connectivity predicted by analytic measures of network communication. *Proceedings of the National Academy of Sciences* **111**, 833–838 (2014).
27. Watson, D. M. & Andrews, T. J. Connectopic mapping techniques do not reflect functional gradients in the brain. *NeuroImage* **277**, 120228 (2023).
28. Warren, D. E. *et al.* Network measures predict neuropsychological outcome after brain injury. *Proceedings of the National Academy of Sciences* **111**, 14247–14252 (2014).
29. Sotiropoulos, S. N. & Zalesky, A. Building connectomes using diffusion MRI: why, how and but. *NMR in Biomedicine* **32**, e3752 (2019).
30. Harnett, M. T., Makara, J. K., Spruston, N., Kath, W. L. & Magee, J. C. Synaptic amplification by dendritic spines enhances input cooperativity. *Nature* **491**, 599–602 (2012).
31. Siletti, K. *et al.* Transcriptomic diversity of cell types across the adult human brain. *Science* **382**, (2023).
32. Paquola, C. *et al.* A multi-scale cortical wiring space links cellular architecture and functional dynamics in the human brain. *PLOS Biology* **18**, e3000979 (2020).
33. Yeh, F. C., Verstynen, T. D., Wang, Y., Fernández-Miranda, J. C. & Tseng, W. Y. I. Deterministic diffusion fiber tracking improved by quantitative anisotropy. *PLoS ONE* **8**, 1–16 (2013).
34. Arnatkevic□iūtė, A., Fulcher, B. D. & Fornito, A. A practical guide to linking brain-wide gene expression and neuroimaging data. *NeuroImage* **189**, 353–367 (2019).
35. Quackenbush, J. Microarray data normalization and transformation. *Nature Genetics* **32**, 496–501 (2002).
36. Hawrylycz, M. *et al.* Canonical genetic signatures of the adult human brain. *Nature Neuroscience* **18**, 1832–1844 (2015).
37. Fulcher, B. D., Little, M. A. & Jones, N. S. Highly comparative time-series analysis: the empirical structure of time series and their methods. *Journal of The Royal Society Interface* **10**, 20130048 (2013).
38. Rubinov, M. & Sporns, O. Complex network measures of brain connectivity: Uses and interpretations. *NeuroImage* **52**, 1059–1069 (2010).
39. Lohmann, G. *et al.* Eigenvector centrality mapping for analyzing connectivity patterns in fMRI data of the human brain. *PLoS ONE* (2010) doi:10.1371/journal.pone.0010232.
40. Bonacich, P. Some unique properties of eigenvector centrality. *Social Networks* **29**, 555–564 (2007).
41. Bertolero, M. A., Thomas Yeo, B. T. & D'Esposito, M. The modular and integrative functional architecture of the human brain. *Proceedings of the National Academy of Sciences of the United States of America* (2015) doi:10.1073/pnas.1510619112.

42. Bullmore, E. & Sporns, O. The economy of brain network organization. *Nature Reviews Neuroscience* **13**, 336–349 (2012).
43. Motter, A. E., Zhou, C. & Kurths, J. Network synchronization, diffusion, and the paradox of heterogeneity. *Physical Review E - Statistical, Nonlinear, and Soft Matter Physics* (2005) doi:10.1103/PhysRevE.71.016116.
44. Arenas, A., Díaz-Guilera, A., Kurths, J., Moreno, Y. & Zhou, C. Synchronization in complex networks. *Physics Reports* **469**, 93–153 (2008).
45. Vos de Wael, R. *et al*. BrainSpace: a toolbox for the analysis of macroscale gradients in neuroimaging and connectomics datasets. *Communications Biology* **3**, 103 (2020).
46. Liu, Z.-Q., Shafiei, G., Baillet, S. & Misic, B. Spatially heterogeneous structure-function coupling in haemodynamic and electromagnetic brain networks. *NeuroImage* **278**, 120276 (2023).
47. Suárez, L. E., Markello, R. D., Betzel, R. F. & Misic, B. Linking Structure and Function in Macroscale Brain Networks. *Trends in Cognitive Sciences* **24**, 302–315 (2020).

Supplemental material

Quantifying the influence of biophysical factors in shaping brain communication through remnant functional networks

Johan Nakuci[1,*], Javier Garcia[1], and Kanika Bansal[1,2,*]

*Corresponding authors' Emails: jnakuci@gmail.com; phy.kanika@gmail.com

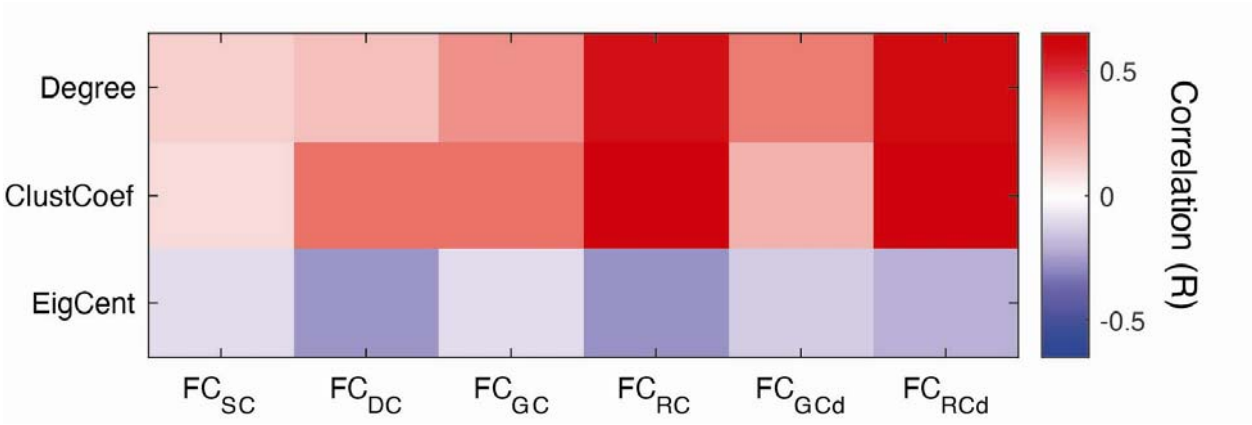

Figure S1. Relationship between biophysical networks and regional network features. The correlations between magnitude of change for each biophysical network across brain regions for weighted degree, clustering coefficient, and eigenvector centrality with strength of the feature. The correlation between FC_{RC} and each of the network features is the same as in Figure 5D and is added for comparative purposes. Unlike RC driven networks, we did not observe a strong correlation between other biophysical networks and weighted degree.

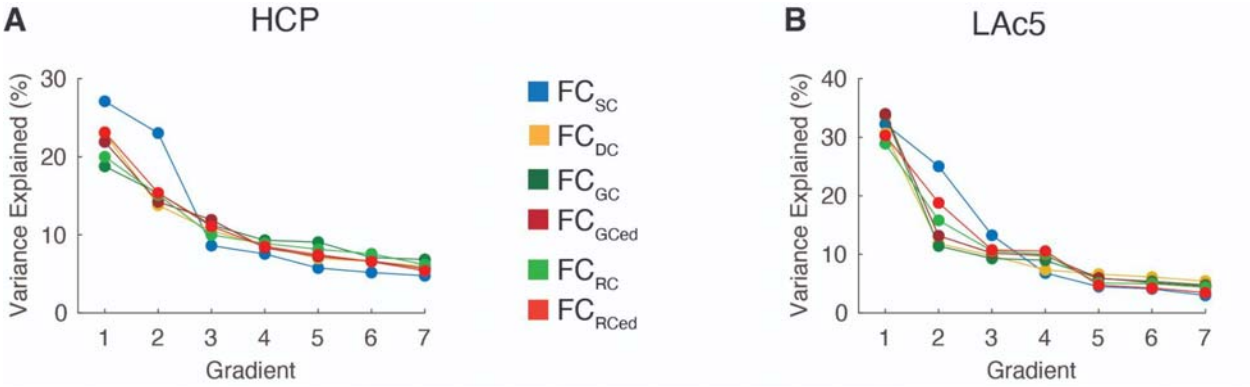

Figure S2. Comparison of the variance explained by the first seven gradients for FC_{Full} and for each of the RFNs. (A) HCP and (B) LA5c datasets. Individual gradients explained comparable amounts of variance among RFNs.

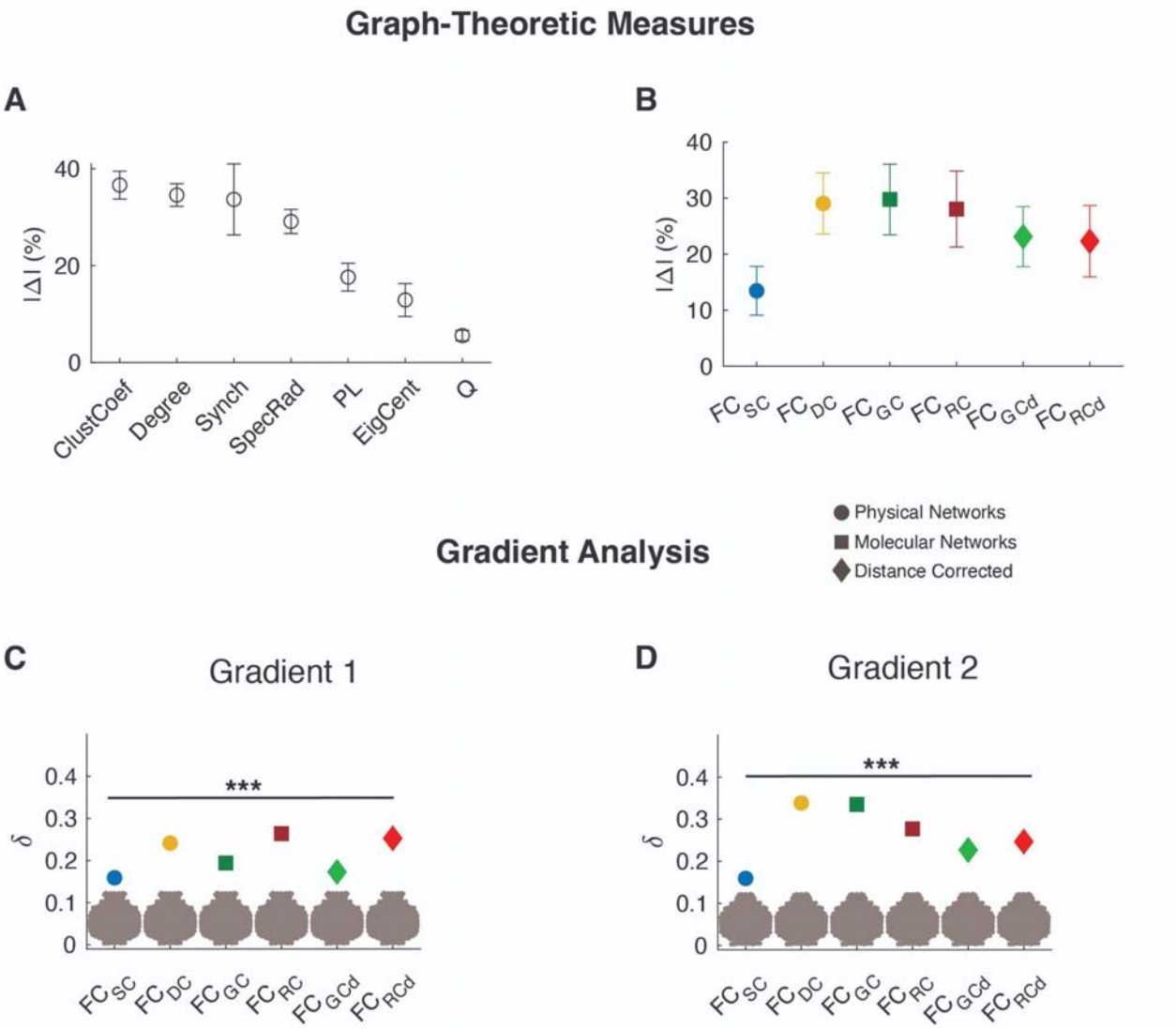

Figure S3. The effect of biophysical networks is not dependent on the sign of connections in FC. (A) Average change (Δ) in graph-theoretic metrics across biophysical networks. Functional connectivity estimated from the HCP dataset were thresholded at zero to remove negative connection prior to estimating graph-theoretic and topological features. Due to the omission of negative edges, we observed changes in network properties when compared to Fig. 3, however, (B) average change for biophysical networks across graph-theoretic metrics shows the dominance of the molecular factors, as discussed in the main paper. (C) Shift in Gradient 1 and(D) shift in Gradient 2 for different RFNs. We calculate the Pearson correlation (R) between the gradient map of FC_{Full} and RFNs and then calculate δ as 1-|R| implying dissimilarity in gradient profiles. The gray dots represent the estimated change – dissimilarity – for the null model which was constructed by removing a set of random connections from the functional connectivity network FC_{Full}. Statistical testing assessed the deviation from the null model with *** denoting p-value < 0.001. We find a significant effect of SC on both the gradients, and the effect of RC is also higher, particularly for Gradient 1, than discussed in Fig. 6. However, the effect of DC is one of the highest across all the biophysical networks, showing its robustness against this methodological choice.

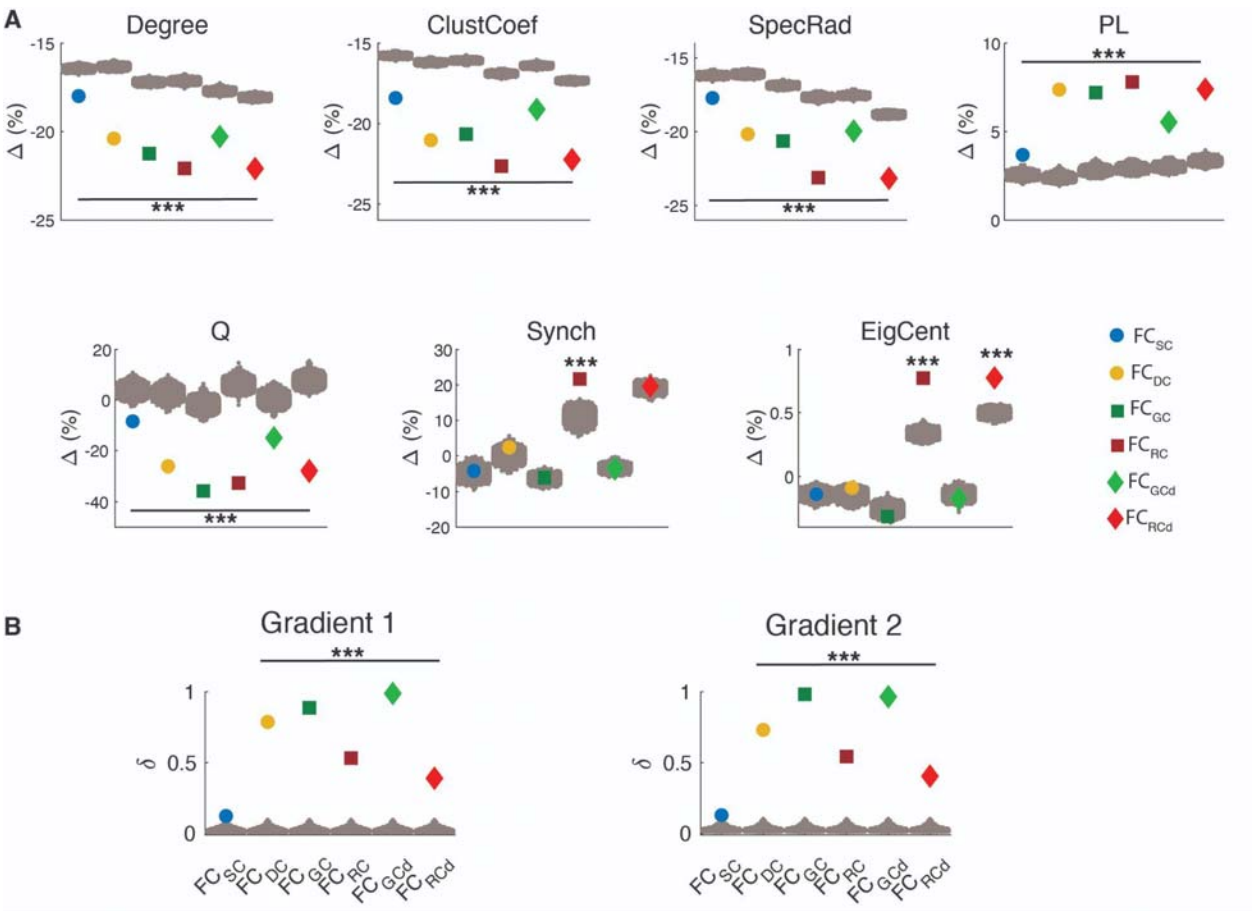

Figure S4. Consistent relationships are obtained when using a null model based on re-wired biophysical networks. (A) Graph-theoretic properties. Weighted Degree (Degree), Clustering Coefficient (ClustCoef), Spectral Radius (SpecRad), Path Length (PL), Modularity (Q), Synchronizability (Synch) and Eigenvector Centrality (EigCent). The effect of each biophysical network was quantified as a percent change (Δ) between FC_{Full} and RFNs for each graph-theoretic measure. Colored dots represent the values after removing SC, DC, GC, RC, GC_d, and RC_d associated connections in the FC_{Full}. (B) Topological properties. Shift in Gradient 1 and Gradient 2 for different RFNs. Given the complexity of the gradient metric, here to estimate the change, we calculate the Pearson correlation (R) between the gradient map of FC_{Full} and RFNs and then calculate δ as 1-|R| implying dissimilarity in gradient profiles. Gray dots represent the values after removing connections in the FC_{Full} from a re-wired, randomized biophysical network (re-wired null model). We generated 1000 total randomized networks for each biophysical network to construct the null distribution. Statistical testing assessed the deviation from the null model with *** denoting p-value < 0.001. Here, we observed a dominance of the molecular factors for the graph-theoretic measures (A) and a dominance of DC and GC associated connectivity for topological features (B), which highlights the robustness of our findings discussed in Figures 4 and 6 for the choice of null model.

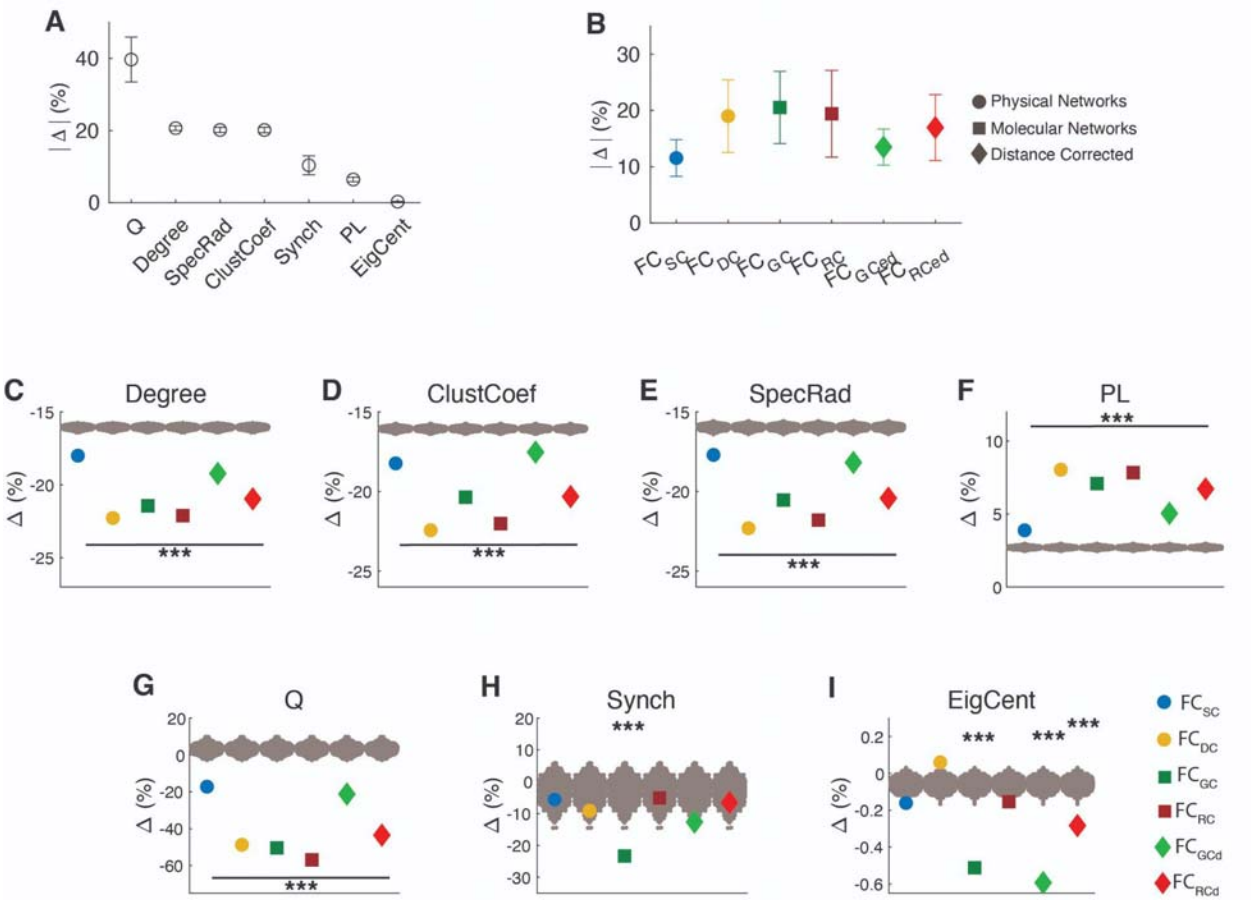

Figure S5. Biophysical networks shaping the graph-theoretical properties of functional brain connectivity in the LA5c dataset. (A) Average change in graph-theoretic metrics across biophysical networks. (B) Average change for biophysical networks across graph-theoretic metrics, highlighting the dominance of RC driven networks. (C) Weighted Degree (Degree), (D) Clustering Coefficient (ClustCoef), (E) Spectral Radius (SpecRad), (F) Path Length (PL), (G) Modularity (Q) , (H) Synchronizability (Synch) and (I) Eigenvector Centrality (EigCent).The effect of each biophysical network was quantified as a percent change (Δ) between FC_{Full} and RFNs for each graph-theoretic measure. Colored dots represent the values after removing SC, DC, GC, GC_d, RC and RC_d associated connections in the FC_{Full}. Gray dots represent the values after removing a random set of connections in the FC_{Full} (null model). FC_{SC}: FC with SC associated connections removed; FC_{DC}: FC with DC connections removed; FC_{GC}: FC with GC connections removed; FC_{RC}: FC with RC connections removed; FC_{GCd}: FC with GC corrected for distance dependencies removed; FC_{RCd}: FC with RC corrected for distance dependencies removed. Statistical testing assessed the deviation from the null model with *** denotinges p-value < 0.001. Replicating the findings discussed in Figures 3 and 4, we observed a clear dominance of the molecular factors (GC and RC) on these graph-theoretic features while the effect of structural connectivity (SC) stays to minimum.

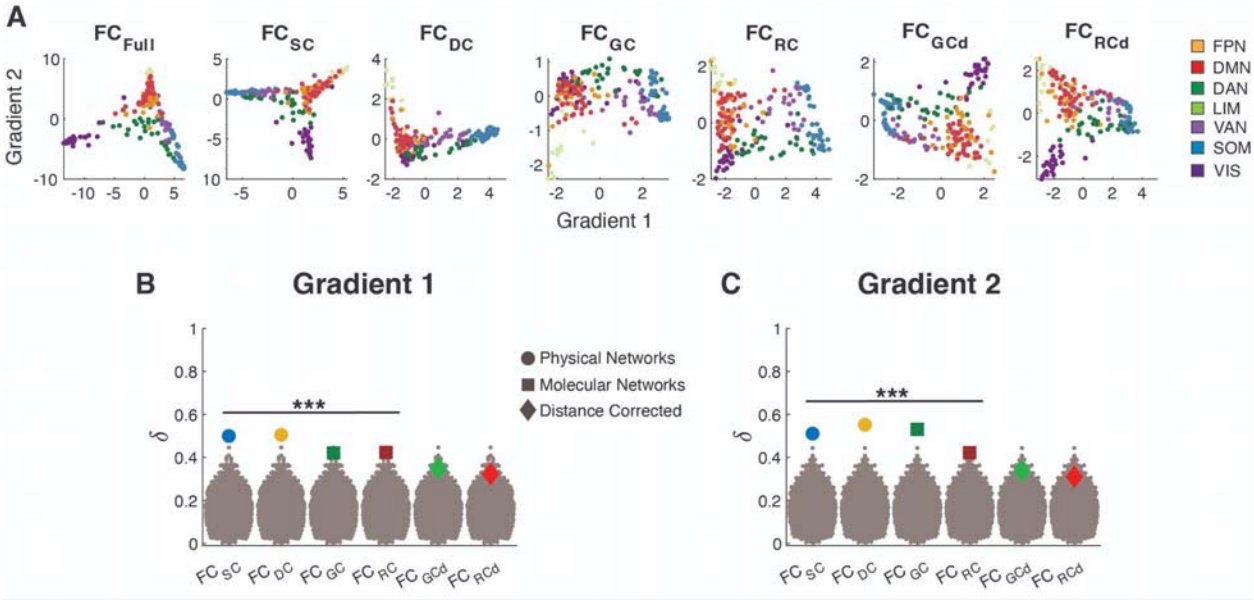

Figure S6. Biophysical networks shape the topological organization of functional brain connectivity in the LA5c dataset. (A) The first two connectivity gradients estimated from the fully connected functional brain network (FC_{Full}), and RFNs, i.e., after removing direct connections associated with SC, DC, GC, GC_d, RC and RC_d. (B) Shift in Gradient 1 and (C) Gradient 2 for different RFNs. Given the complexity of the gradient metric, here to estimate the change, we calculate the Pearson correlation (R) between the gradient map of FC_{Full} and RFNs and then calculate δ as 1-|R| implying dissimilarity in gradient profiles. The gray dots represent the estimated change – dissimilarity – for the null model which was constructed by removing a set of random connections from the functional connectivity network FC_{Full}. Note that there was a significant effect of SC on topological gradients, unlike what was observed in HCP data (Fig. 6). Similarly, while DC and GC emerge as dominant factors impacting Gradient 2, the effect of molecular factors on Gradient 1 is lower than both the physical factors (SC and DC). LA5c included a shorter scan length (~ 5 minutes) than HCP (~ 15 minutes), and some of these differences may reflect that, however, the impact of molecular factors on Gradient 1 seems more nuanced across different robustness tests we performed and requires further testing. Nonetheless, the dominant effect of DC is robustly observed across both the gradients for different methodological and data choices considered in this study. FPN, Frontoparietal Network; DMN, Default Mode Network; DAN, Dorsal Attention Network; LIM, Limbic; VAN, Ventral Attention Network; SOM. Statistical testing assessed the deviation from the null model with *** denoting p-value < 0.001.

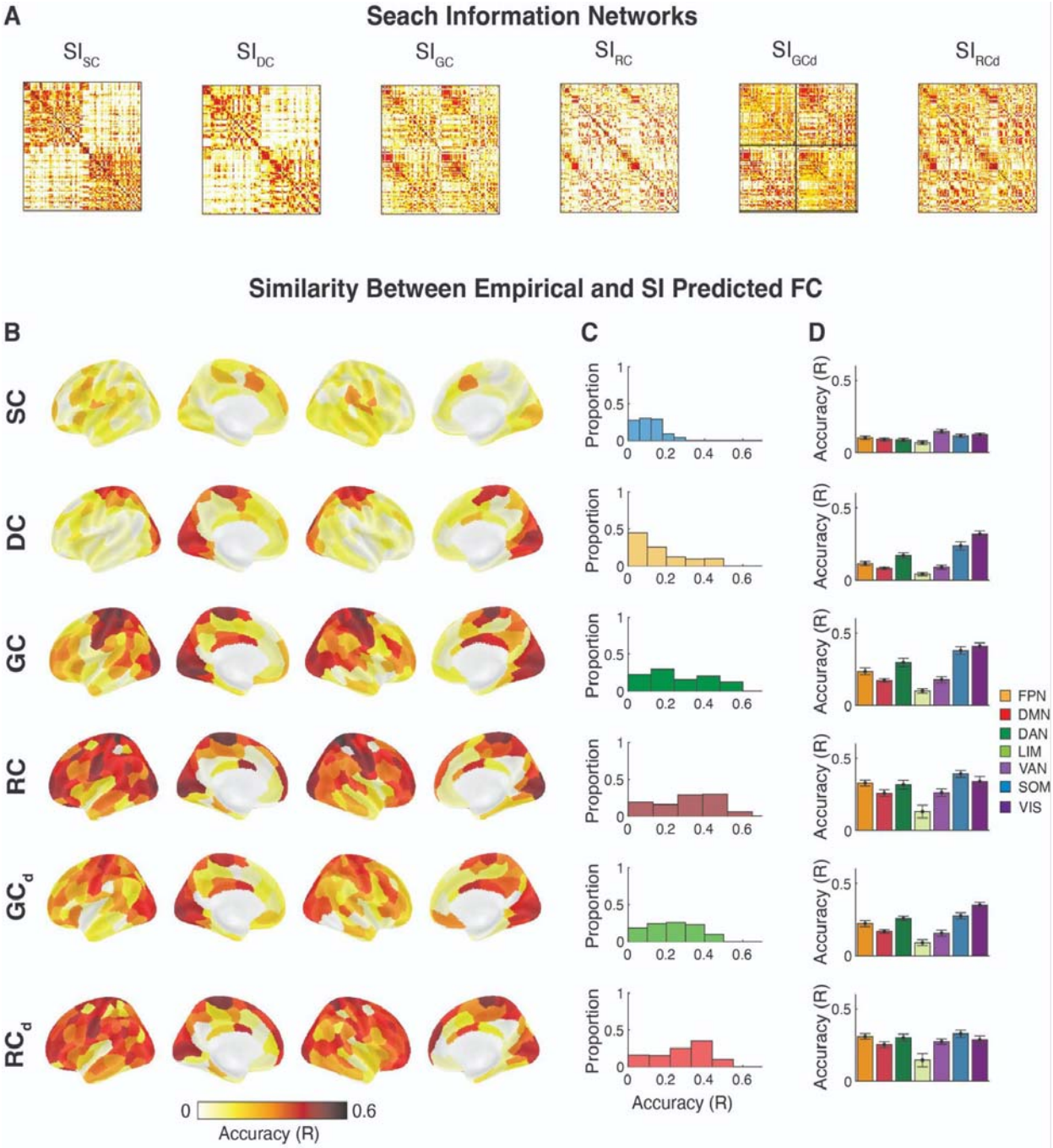

Figure S7. Modeling the functional connectivity from biophysical networks in the HCP dataset. (A) Most previous work has focused on modeling on understanding how anatomical wiring constraints and shapes communication[47]. We extend the modeling of FC from biophysical factors using Search Information (SI)[26]. SI measures the amount of information required to traverse the shortest paths between a given pair of brain regions and it has been shown to be a good model for predicting FC. The SI based *predicted* functional connectivity was derived from each of the biophysical networks – SC, DC, GC, GC_d, RC and RC_d. (B) Accuracy of SI predicted functional connectivity for each brain region. The biophysical networks exhibited differential capabilities in predicting FC (panel B). On average the best predictor of nodewise functional connectivity were RC ($R = 0.31 \pm 0.16$; $P < 0.001$) and RC_d ($R = 0.28 \pm 0.13$; $P < 0.001$). In fact, for 84 out of 200 ROIs (42%), RC was the best predictor of FC. Accuracy was quantified

at the similarity, Pearson correlation (R), of the regional connectivity profile between the SI predicted and empirical functional connectivity (FC_{Full}) of each of the 200 brain regions. (C) Distribution of accuracy values among biophysical networks. (D) The average performance within large-scale functional communities. RC and RC_d exhibited similar predictive capabilities across the cortex and large-scale brain networks suggesting neuroreceptor congruence uniformly shapes FC across the cortex.Whereas, the other biophysical networks exhibited localized predictive capabilities. The predictive capabilities of DC, GC and GC_D were primarily constrained to the somatomotor and visual networks (panel D). On the other hand, SC weakly predicted functional connectivity across the brain. FPN, Frontoparietal Network; DMN, Default Mode Network; DAN, Dorsal Attention Network; LIM, Limbic; VAN, Ventral Attention Network; SOM, Somatomotor; VIS, Visual Network.

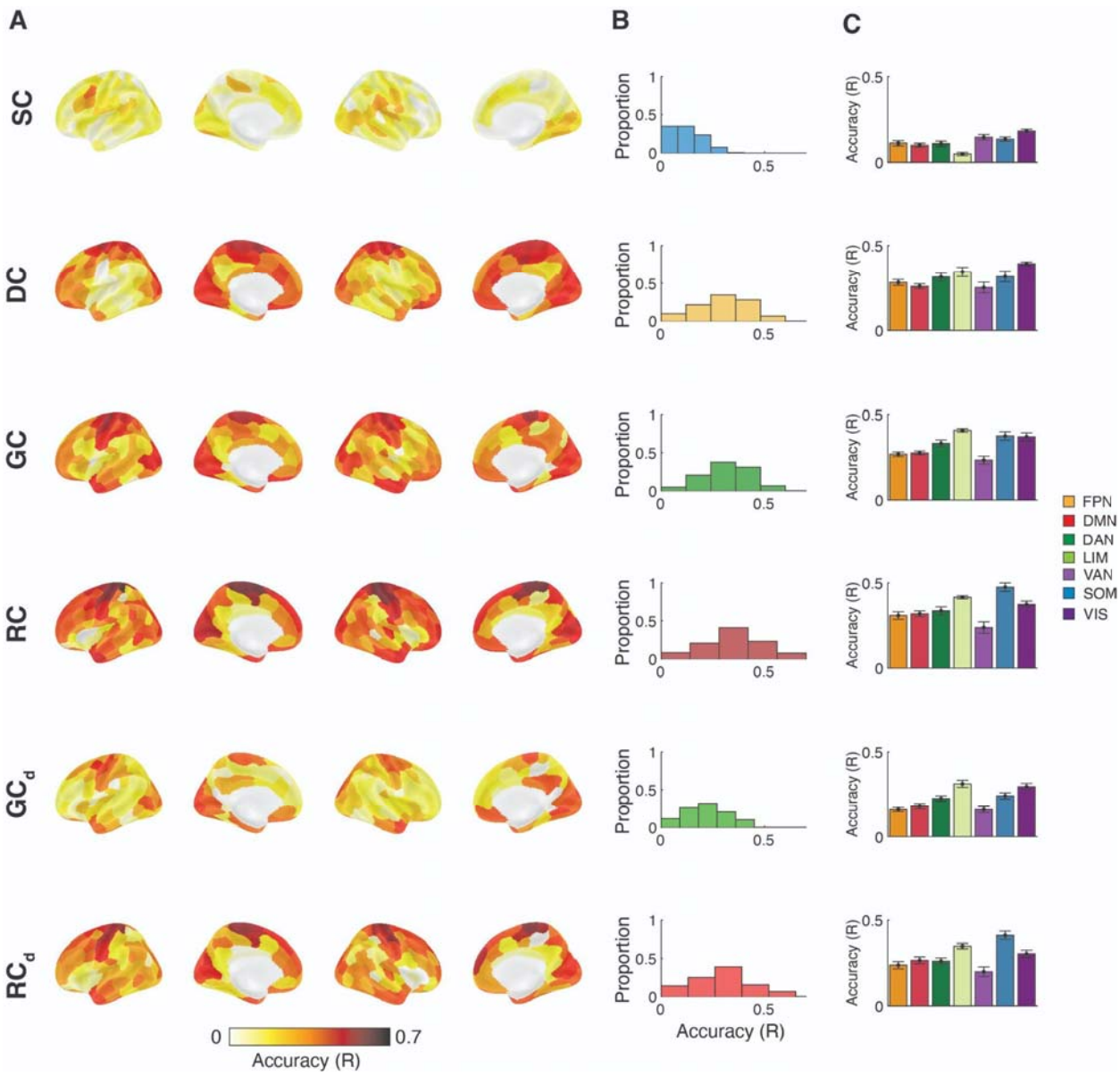

Figure S8. Modeling the functional connectivity from biophysical networks in the LA5c dataset. (A) Performance of SI predicted functional connectivity for each brain region. Performance was estimated with a linear model to compare the similarity in the regional connectivity profile between the SI predicted and empirical functional connectivity of each of the 200 brain regions. (B) Distribution of accuracy scored in modeling FC among biophysical networks. (C) The average performance within large-scale functional communities. These findings are aligned with the findings presented in the Fig. S7 for HCP. FPN, Frontoparietal Network; DMN, Default Mode Network; DAN, Dorsal Attention Network; LIM, Limbic; VAN, Ventral Attention Network; SOM, Somatomotor; VIS, Visual Net